

SLAC-PUB-470  
July 1968  
(EXP)

Compilation of  $\pi^- p$  Data at 4 GeV/c: Backward Resonance  
Production and  $\pi\pi$  Scattering<sup>†</sup>

NOTRE DAME-PURDUE-SLAC Collaboration

P. B. Johnson, J. A. Poirier, N. N. Biswas, N. M. Cason,  
T. H. Groves, V. P. Kenney, J. T. McGahan, and W. D. Shephard,

Department of Physics, University of Notre Dame, Notre Dame, Indiana  
and

L. J. Gutay, J. H. Campbell, R. L. Eisner, F. J. Loeffler,  
R. E. Peters, R. J. Sahni, and W. L. Yen

Department of Physics, Purdue University, Lafayette, Indiana  
and

I. Derado and Z. G. T. Guiragossian

Stanford Linear Accelerator Center, Stanford University, Stanford, California

(Submitted to Physical Review)

---

<sup>†</sup> Work supported in part by the Atomic Energy Commission  
and the National Science Foundation.

Abstract

In  $\pi^-p$  single-pion-production reactions near 4 GeV/c we observe several interesting features. Backward  $\rho^0$  production is seen to occur with  $d\sigma/du = 63 \pm 21 \mu\text{b}/(\text{GeV}/c)^2$  at  $180^\circ$ . Backward  $\rho^-$  production is less prominent. We see evidence for production at small  $u$  of  $N^{*0}$  ( $p\pi^-$  near 1700 MeV),  $\Delta^-$  ( $n\pi^-$  at 1236 MeV) and possible evidence for other  $n\pi^-$  structure at about 1800 MeV. The density-matrix elements for peripheral  $\rho^0$  production are presented in the Jackson and in the helicity frames. The  $\pi^+\pi^-$  elastic cross section is obtained by extrapolation of the data to the mass shell. The S-wave  $\pi\pi$  phase shifts are calculated by two methods and compared with previous results. We find evidence in the dipion decay angular distribution for the  $\pi^+\pi^-$  decay mode of the  $S^*(1070)$ .

## I. INTRODUCTION

The results presented here are obtained from a study of single pion production in  $\pi^-p$  interactions at incident momenta of 3.65, 3.90, 4.0, and 4.16 GeV/c.<sup>1</sup> The weighted average incident momentum is 4.0 GeV/c. We have 7916 events of the type



and 4978 events of the type



The weighted total cross sections are  $3.12 \pm .05$  mb for reaction (1) and  $2.10 \pm .04$  mb for reaction (2). Reactions (1) and (2) at these energies are dominated by peripheral  $\rho^0$ ,  $f^0$ , and  $\rho^-$  production. Isobar production has been observed to occur about 8% of the time in reaction (1) and 20% in reaction (2).<sup>1</sup>

We examine the following three important characteristics of the above reactions: backward resonance production,  $\rho$  production and decay, and  $\pi\pi$  scattering. In section II we discuss u channel production of resonances. In section III  $\rho$  and  $f^0$  production and decay are discussed. The  $\rho$ -decay density-matrix elements are given in both the Jackson frame, in which the quantization axis is the incident  $\pi^-$  direction, and the helicity frame, in which the quantization axis is the  $\rho$  line of flight. In section IV we analyze the peripherally produced dipion events

in terms of  $\pi\pi$  scattering. In discussing angular distributions we will use the convention that  $\theta_{ab}^*$  refers to the angle between incoming particle a and outgoing particle b in the overall center-of-mass system and  $\theta_{ab}$  refers to the angle between incoming particle a and outgoing particle b in the appropriate two-particle rest system.

## II. U-CHANNEL RESONANCE PRODUCTION

Figure 1 shows the  $\pi^+\pi^-$  effective mass distributions for events in which the dipion system is produced in the backward hemisphere, i. e.,  $\cos \theta_{pn}^* < 0$ . The shaded histogram is the subsample with  $\cos \theta_{pn}^* < -0.6$ . We see a clear  $\rho^0$  signal above background for both selection criteria; in contrast, we see no significant evidence for  $f^0$  or any other structure for  $\cos \theta_{pn}^* < -0.6$ . Using a smooth background for this mass spectrum and correcting for losses in the tails of a Breit-Wigner curve for the  $\rho^0$  intensity, we estimate the  $\rho^0$  production cross section to be  $87 \pm 15 \mu\text{b}$  for backward production ( $\cos \theta_{pn}^* < 0$ ).

From the mass spectra shown in Fig. 1, we estimate that about 50% of the events in the  $\rho^0$  region are background; within statistics, this fraction is independent of  $\cos \theta_{pn}^*$  in the interval  $-0.3 \leq \cos \theta_{pn}^* < -1.0$ . Thus, we have calculated the differential cross section for the backward region using the number of events in the  $\rho^0$  region and the total cross section

of  $87 \mu\text{b}$  as mentioned before. Figure 2 shows the center-of-mass  $\rho^0$  angular distribution. The differential cross section seems to rise in the backward direction although the hypothesis of constant cross section is consistent with the data (at the 20% confidence level). We estimate the  $\rho^0$  differential cross section near  $180^\circ$  to be  $63 \pm 21 \mu\text{b}/(\text{GeV}/c)^2$ .

The production mechanism for  $\rho^0$  in the backward direction is a topic of some interest. In Fig. 3 we have plotted the dipion decay angular distribution for three different production regions. In the forward region,  $\cos \theta_{pn}^* > 0.6$ , the distribution in  $\theta_{\pi\pi^-}$  shows the  $\cos^2 \theta_{\pi\pi^-}$  contribution from one-pion-exchange and a strong forward asymmetry. In contrast the decay distributions for  $\cos \theta_{pn}^* < 0.6$  show no asymmetry and are consistent with isotropy. If baryon exchange contributes to backward production, the  $\rho$  is produced at the proton vertex; in this case the quantization axis becomes the incident proton direction. The resulting distributions in  $\cos \theta_{p\pi}$  and  $\phi_{p\pi}$  for  $\cos \theta_{pn}^* < -0.6$  are shown in Fig. 4. Both of these distributions are consistent with isotropy. To examine effects on these distributions due to background present under the  $\rho$  peak, we have looked at the corresponding distributions for events on both sides of the  $\rho$ . The distributions of Fig. 4(a) and 4(b) are not altered after subtraction of

these background distributions. These results are consistent with predictions for exchange of an unpolarized nucleon.

In reactions (1) and (2), if backward  $\rho$  production is interpreted in terms of a Reggeized baryon-exchange model, the  $N_\alpha$ ,  $N_\gamma$ , and  $\Delta$  trajectories can all contribute to  $\rho^0$  production whereas only  $\Delta$  exchange can contribute to  $\rho^-$  production. In Fig. 5 we show the  $\pi^0\pi^-$  effective mass distribution for events with  $\cos \theta_{pp}^* < -0.6$ . We estimate the  $\rho^-$  signal to be  $18 \pm 5$  events; this corresponds to about 1/4 the  $\rho^0$  signal seen in the shaded distribution of Fig. 1. This suggests that  $\Delta$  exchange is weaker than nucleon exchange for backward  $\rho$  production. When we look at the production angular distribution for the  $\pi^-\pi^0$  system in Fig. 6, we observe a sharp increase in the differential cross section at the last bin ( $\cos \theta_{pp}^* < -0.96$ ) which suggests  $\Delta^{++}$  exchange. However, we are not able to associate this peaking with resonance production in the dipion system.

Figure 7(a) shows the neutron  $\pi^-$  effective mass spectrum for events which have  $\cos \theta_{\pi^-\pi^+}^* < -0.6$  and which lie outside the  $\rho^0$  band (0.70 to 0.85 GeV). We observe a strong  $\Delta_{1236}^-$  signal and possible evidence for other structure at 1.80 and 1.96 GeV. Both of these latter enhancements are two- to three-standard deviation effects. The steeply rising

background in Fig. 7(a) comes from events in which the dipion system is peripherally produced. We can effectively suppress this background by making cuts in  $\cos \theta_{pn}^*$ ; the shaded events in Fig. 7(a) are removed when  $\cos \theta_{pn}^* < 0.9$ . (The two enhancements remain significant even when we make the more stringent cut  $\cos \theta_{pn}^* < 0.8$ .) In Fig. 7(b) the corresponding spectrum is shown for the middle region  $-0.6 < \cos \theta_{\pi^-\pi^+}^* < 0.6$ . We note that the  $\Delta_{1236}^-$ , the 1.80, and 1.96 GeV enhancements are not present. We suggest that these enhancements are not due to any known background effects and that they may be interpreted as I-spin 3/2 isobars. Studies of the decay distributions are not statistically significant. Phase-shift analyses<sup>2</sup> have reported evidence for several new I = 3/2 isobars not previously seen, including a  $P_{31}$  resonance at 1.934 and a  $D_{35}$  at 1.954 GeV. However, there is no reported structure at 1.80 GeV in the phase-shift analyses.

The other system for which nucleon exchange is allowed is the  $p\pi^-$  combination. The  $p\pi^-$  effective mass is plotted in Fig. 8 for  $\cos \theta_{\pi^-\pi^0}^* < -0.6$ . We observe a signal near 1.68 GeV where several I = 1/2 isobars have been reported. There is no evidence for a 1.80 or 1.96 GeV enhancement, but this is not unexpected since the Clebsch-Gordan coefficient is unfavorable for producing I = 3/2 systems. In contrast to the above, the backward  $n\pi^+$  and  $p\pi^0$  systems require doubly charged isobar

exchange in the u channel. The mass spectra for these systems, Figs. 9 and 10, show no interesting structure. Thus we conclude that within the limits of our statistics isobar production, like boson production, proceeds predominantly via nucleon exchange.

### III. $\pi\pi$ RESONANCES

Figure 11 shows the invariant mass spectrum for reaction (1) for all the data; the shaded histogram shows events with  $\cos^* \theta_{pn} \geq 0.94$ , a cut which, for a dipion mass of 0.775 GeV, corresponds to  $|t| < 0.2 \text{ (GeV/c)}^2$ . The  $\rho^0$  and  $f^0$  resonances are prominent: about 40% of the events correspond to  $\rho^0$  production and 14% to  $f^0$  production. The solid curve in Fig. 11 is a fit to the data assuming two constant-width Breit-Wigner shapes for the  $\rho^0$  and the  $f^0$  plus phase space for the background. More details of the fitting procedure and the values of the fitted parameters are discussed below.

Figures 12(a) and 12(b) show two Dalitz plots for reaction (1); two plots are shown since the third two-particle effective mass for a point is dependent on the incident momentum.

Figure 13 is a Chew-Low scatter plot of  $M(\pi^+\pi^-)$  versus  $\sqrt{-t/\mu^2}$  for reaction (1) where  $\mu$  is the pion mass. There is a strong concentration of events near the minimum allowable momentum transfer. There is also some increase in the density of events near the maximum allowable momentum transfer; these events

have been discussed in section II.

Figure 14 is a scatter plot of  $\cos \theta_{\pi^+\pi^-}$  versus the  $\pi^+\pi^-$  invariant mass. The strong forward-backward asymmetry for the  $\rho^0$  region is apparent; the distribution is rather symmetrical in the  $f^0$  region but becomes quite sharply peaked near  $\cos \theta = +1.0$  for masses above the  $f^0$ . The cluster of events near  $\cos \theta_{\pi^+\pi^-} = \pm 1$  at 1.0 GeV will be discussed in section IV.

Table I summarizes various maximum likelihood fits to the mass spectrum in Fig. 11. We have used various forms of the expected Breit-Wigner shapes:<sup>3</sup>

$$BW = A \frac{\Gamma}{2} F / ((M - M_0)^2 + (\Gamma/2)^2) \quad (3)$$

and

$$BW = A \Gamma F / ((M^2 - M_0^2)^2 + M^2 \Gamma^2) \quad (4)$$

where A is the intensity, F is a function defined in Table I,  $M_0$  is the resonance mass, and  $\Gamma$  is the full width at half maximum for the resonance. The overall fit function is

$$dN/dM = PS (1.0 + BW_{\rho} + BW_f) \quad (5)$$

where PS is three-body phase space. Fit errors are shown for fit number 4; the other fits have comparable errors. Note that the fraction of  $\rho^0$  varies from 0.340 to 0.404 depending on the function used.

If one takes the average ( $\rho^0/\text{total} = 0.377$ ) the total  $\rho^0$  production cross section at 4 GeV/c falls in the range 1.06 to 1.26 mb based on the fits in Table I. Figure 15 shows the  $t$ -distribution for  $\rho^0$  production scaled so that the total cross section is 1.15 mb; the shape of the distribution is obtained from all events with effective dipion mass in the interval 0.70-0.85 GeV. From the fits we estimate that this mass interval contains 18% non-rho background.

In Fig. 16 we show a scatter plot of  $\cos \theta_{\pi\pi}$  versus the Treiman-Yang angle together with the projections on the axes. The non-uniform distribution of events on this scatter plot has been fitted with a function parameterized by density matrix elements  $\rho_{mn}$  which includes possible S- and P-wave interference effects.<sup>4</sup> The  $t$ -dependence of these matrix elements is presented in Figs. 17 and 18.

Interest in the vector dominance model has focused attention to the density matrix elements in the dipion helicity frame. We have evaluated the density-matrix elements in the helicity frame as a function of  $t$ ; the results of the fits are shown in Figs. 19 and 20.

#### IV. $\pi\pi$ SCATTERING

It has been observed previously<sup>1</sup> that  $\rho^0$  production and decay can be fairly well explained for small values of  $|t|$  by

models based on one-pion-exchange, e. g., the absorption model<sup>5</sup> (c. f. Figs. 17 and 18). We have also seen in Fig. 13 that reaction (1) is peripheral not only in the  $\rho^0$  and  $f^0$  resonance bands but across the entire dipion mass spectrum. Similar observations have been made in other experiments.<sup>6</sup> Thus there is considerable evidence suggesting that for small  $|t|$  the dipion decay angular distributions from reaction (1) contain information related to  $\pi\pi$  elastic scattering. The question of obtaining the S-wave  $\pi\pi$  phase shifts from data on reactions (1) and (2) is a topic of current concern.

Gutay et al.<sup>7</sup> observed that the  $t$  dependence of the dipion decay distribution was fitted rather well by an absorption model calculation which included S-wave amplitudes. Applying this model to data from reaction (1) at 2.7 GeV/c they obtained two sets of  $I = 0$  S-wave phase shifts. The same model was applied to slightly more than half the data in the present collaboration and the results were in quite good agreement with those obtained previously.<sup>4</sup> It should be pointed out that in the calculation of the  $\pi\pi$  S-wave phase shifts one encounters two types of ambiguities. An unavoidable ambiguity results from the invariance of the scattering amplitude ( $\alpha e^{i\delta} \sin \delta$ ) under the transformation  $\delta \rightarrow \delta \pm n\pi$ . The second ambiguity, in analyses based on S- and P-wave interference, arises from the invariance of the interference term under the transformation  $\delta_0^0 \rightarrow \pi/2 -$

$(\delta_0^0 - \delta_1^1)$ .<sup>7</sup> Here  $\delta_J^I$  denotes the phase shift for isospin I and angular momentum J.

In the present collaboration, we have calculated the isoscalar S-wave  $\pi\pi$  phase shifts from the asymmetry parameter

$$g = \frac{F-B}{F+B} \quad (6)$$

where F is the number of events with  $\cos \theta_{\pi\pi} > 0$  and B is the number of events with  $\cos \theta_{\pi\pi} < 0$ . When the dipion angular distribution was fitted to the form

$$U(\theta, m, t) = a(m, t) + b(m, t) \cos \theta + c(m, t) \cos^2 \theta \quad (7)$$

it was observed<sup>4, 7</sup> that the ratio b/c was effectively independent of t and a/c was strongly dependent on t. In terms of (7) the asymmetry is

$$g = \frac{b/c}{2/3 + 2 a/c} \quad (8)$$

In Fig. 21 we show g as a function of  $m_{\pi\pi}$  for  $|t| < 0.2 \text{ (GeV/c)}^2$ . We have assumed b/c to be independent of t consistent with the results of Refs. 4 and 7.

The phase shifts  $\delta_0^0$  are obtained by solving the equations

$$\tan \delta_1^1 = \frac{\sin 2\delta_0^0}{3g \frac{\alpha(\delta_0^0, \delta_0^2)}{\beta(\delta_0^0, \delta_0^2)} - 2 \sin^2 \delta_0^0} \quad (9)$$

where

$$\alpha = 1 + k \left[ \frac{4 \sin^2 \delta_o^o + \sin^2 \delta_o^2 + 4 \cos (\delta_o^o - \delta_o^2) \sin \delta_o^o \sin \delta_o^2}{27 \sin^2 \delta_1^1} \right] \quad (10)$$

and

$$\beta = 1 + \left[ \frac{\cos (\delta_o^2 - \delta_1^1) \sin \delta_o^2}{2 \cos (\delta_o^o - \delta_1^1) \sin \delta_o^o} \right] \quad (11)$$

The values of  $\delta_1^1$  used in (9) are from a relativistic calculation.<sup>8</sup> The values of  $\delta_o^2$  were taken from Baton et al.<sup>9</sup> The parameter  $k$  in (10) is the correction introduced by the  $t$  dependence of  $a/c$  and was varied between 1.0 and 0.25; these limits were suggested by the results cited above<sup>7</sup> based on an absorption model. The dependence of the solution  $\delta_o^o$  on  $k$  was treated as part of the uncertainty in  $\delta_o^o$ .

In Fig. 22 we show the calculated  $\delta_o^o$  as a function of  $M(\pi, \pi)$  together with some results reported by other groups. The sets labeled I and II are related to each other by the interference term ambiguity. Set III is shifted by  $180^\circ$  from Set I. The results of Walker et al.<sup>10</sup> were obtained by a method similar to that of Ref. 7 except that a constant correction factor was applied to the data to account for absorption effects. The set of  $\delta_o^o$  preferred by Walker et al. is seen to be in qualitative agreement with Set II. Malamud and Schlein<sup>11</sup> fitted the dipion-decay angular distribution

in the  $\rho$  helicity frame to obtain the S-wave phase shifts. We see that the set of  $\delta_0^0$  preferred by Malamud and Schlein is in good agreement with Set I in Fig. 22. A recent determination of  $\delta_0^0$  at low  $M(\pi, \pi)$  from interference between Coulomb and strong interaction amplitudes<sup>12</sup> is consistent with Sets I and III.

It is of interest to apply the Bander, Shaw, and Fulco model,<sup>13</sup> which includes one-pion-exchange with absorption in the initial and final states to our data for reaction (1). Figure 23 shows the result of such an analysis based on scattering length, effective range, and resonance width parameters suggested by Bander.<sup>14</sup> The  $I = 2$  S-wave phase shift  $\delta_0^2$  has been obtained from Ref. 9. It is found that this evaluation of  $\pi\pi$  phase shifts is primarily sensitive to variations in the value of the  $\rho$  meson width. The S-wave  $I = 0$  phase shift  $\delta_0^0$  solution thus obtained is found to be in qualitative agreement with that of Set II of Fig. 22. In Fig. 24 we show the forward-backward  $\pi\pi$  asymmetry ratio for  $t_{\min} < |t| < 0.06 \text{ (GeV/c)}^2$  and for  $0.06 < |t| < 0.2 \text{ (GeV/c)}^2$ , together with the predictions of this phase-shift analysis. The agreement is found to be adequate.

In principle, the  $\pi\pi$  elastic cross section and phase shifts can be determined from a Chew-Low extrapolation.<sup>15</sup> Such a procedure has been used recently by Baton et al. to obtain the  $\rho^-$  parameters and the  $I = 2$  S-wave phase shift.<sup>9</sup> We have performed the extrapolation to obtain the  $\pi^+\pi^-$  cross section; the

results are presented in Fig. 25. The cross section passes through the limits  $12\pi\kappa^2$  for P-wave and  $(80/9)\pi\kappa^2$  for D-wave scattering near 0.77 and 1.25 GeV as expected for the  $\rho^0$  and  $f^0$  resonances. Our statistics, however, do not permit an accurate determination of the S-wave phase shifts from such an extrapolation.

The  $\pi^+\pi^-$  and  $\pi^0\pi^-$  decay angular distributions have been fitted to a Legendre polynomial expansion of the form

$$1 + \left[ 1/A_0(m_{\pi\pi}) \right] \sum_{j=1}^{10} A_j(m_{\pi\pi}) P_j(\cos \theta_{\pi\pi}) . \quad (12)$$

The first four terms of these expansions are shown in Fig. 26 for reaction (1) and Fig. 27 for reaction (2). In almost all cases higher order terms were consistent with zero. For reaction (1) only events with  $|t| < 0.2 \text{ (GeV/c)}^2$  were included in the fits; the cutoff for reaction (2) was  $|t| < 0.4 \text{ (GeV/c)}^2$ . Notice that for the  $\pi^+\pi^-$  data the  $A_1/A_0$  term in Fig. 26 is large and positive throughout the  $\rho^0$  region, goes through a maximum at about 0.92 GeV, and falls off to a minimum close to zero near 1.07 GeV. In the  $\pi^0\pi^-$  final state the  $A_1/A_0$  term is small and negative from 0.5 to 0.8 GeV and increases rapidly with dipion energy above 0.8 GeV. The energy dependence of  $A_2/A_0$  for the  $\pi^+\pi^-$  final state shows a peak near 1.03 GeV. This structure ( $\sim$  three standard deviations) is not seen in the  $\pi^0\pi^-$  data. This structure

in  $A_2/A_0$  near 1.03 GeV is also visible in the scatter plot of  $M(\pi^+\pi^-)$  vs.  $\cos \theta_{\pi\pi}$ , as seen in Fig. 14. The peaking of  $A_2/A_0$  together with an increasing  $A_1/A_0$  for  $m_{\pi\pi} > 1.0$  GeV is consistent with constructive interference between a rapidly increasing  $\delta_0^0$  and an increasing D-wave phase shift,  $\delta_2^0$ , although we are not able to rule out the possibility that the effect is due to D or higher partial waves. This is compatible with the suggestion of a resonance near 1.05 GeV<sup>16</sup> such as the  $S^*$  reported in the  $K\bar{K}$  system.

A quantitative interpretation of the coefficients in Figs. 26 and 27 should be approached with some caution. Near the  $\rho^0$  mass  $A_2/A_0$  has a maximum value of 1.3 instead of 2.0 as expected for pure P-wave scattering.<sup>17</sup> This indicates the importance of absorption effects. Furthermore, in the same mass region  $A_2/A_0$  for  $\pi^0\pi^-$  is roughly a factor of two smaller than for  $\pi^+\pi^-$ . This discrepancy seems to be due to vector exchange in  $\rho^-$  production which is significant near 4 GeV/c.<sup>18</sup> It was pointed out above that an expansion of the angular distribution in powers of  $\cos \theta_{\pi\pi}$ , Eq. (7), proved particularly useful for phase shift calculations because the ratio  $b/c$  was found to be independent of  $t$ . The terms in expression (12) are found to be strongly  $t$ -dependent. In Fig. 28 we show the results of extrapolating the Legendre coefficients  $A_1/A_0$  and  $A_2/A_0$  to the pion pole. The

curves are least-squares fits to a quadratic form in  $t$ . Both coefficients are seen to depend strongly on  $t$  and the values at the pole have large errors associated with them.

We suggest that it is highly desirable to extend S-wave  $\pi\pi$  phase-shift calculations to dipion masses greater than 900 MeV. A phase-shift analysis offers the best means of settling questions about possible resonances between the  $\rho^0$  and  $f^0$ . Also, it would help determine which of Sets I and II is the correct set for  $\delta^0$  since Set I approaches  $180^\circ$  and Set II is near  $90^\circ$  at 900 MeV.

REFERENCES

- <sup>1</sup> Y. Y. Lee, B. P. Roe, D. Sinclair, and J. C. Vander Velde, Phys. Rev. Letters 12 , 342 (1964) (3.65 GeV/c); R. W. Birge, R. R. Ely, T. S. Schuman, Z. G. T. Guiragossian, and M. Whitehead, Proceedings of the Twelfth International Conference on High Energy Physics (Dubna, 1964) p. 153; Aachen-Birmingham-Bonn-Hamburg-London (I. C.)-Munich Collaboration, Nuovo Cimento 31 , 729 (1964) (4.0 GeV/c); I. Derado, V. P. Kenney, J. A. Poirier, and W. D. Shephard, Phys. Rev. Letters 14 , 872 (1965) (4.0 GeV/c); R. L. Eisner, P. B. Johnson, P. R. Klein, R. E. Peters, R. J. Sahni, W. L. Yen, and G. W. Tautfest, Phys. Rev. 164 , 1699 (1967) (4.16 GeV/c).
- <sup>2</sup> P. Bareyre, C. Bricman, and G. Villet, Saclay preprint (1967); C. H. Johnson, P. D. Grannis, M. J. Hansroul, O. Chamberlain, G. Shapiro, and H. M. Steiner, UCRL-17683 (1967); A. Donnachie, R. G. Kirsopp, and C. Lovelace, CERN preprint TH838 (1967).
- <sup>3</sup> J. D. Jackson, Nuovo Cimento 34 , 1644 (1964).
- <sup>4</sup> P. B. Johnson, L. J. Gutay, R. L. Eisner, P. R. Klein, R. E. Peters, R. J. Sahni, W. L. Yen, and G. W. Tautfest, Phys. Rev. 163 , 1497 (1967).
- <sup>5</sup> K. Gottfried and J. D. Jackson, Nuovo Cimento 34 , 735 (1964); L. Durand III and Y. T. Chiu, Phys. Rev. 139 , B646 (1965).

- 6 J. D. Jackson, Rev. Mod. Phys. 37 , 484 (1965); D. H. Miller, L. Gutay, P. B. Johnson, F. J. Loeffler, R. L. McIlwain, R. J. Sprafka, and R. B. Willmann, Phys. Rev. 153 , 1423 (1967).
- 7 L. J. Gutay, P. B. Johnson, F. J. Loeffler, R. L. McIlwain, D. H. Miller, R. B. Willmann, and P. L. Csonka. Phys. Rev. Letters 18 , 142 (1967).
- 8 J. S. Ball and M. Parkinson, Phys. Rev. 162 , 1509 (1967).
- 9 J. P. Baton, G. Laurens, and J. Reignier, Phys. Letters 25B , 419 (1967).
- 10 W. D. Walker, J. Carroll, A. Garfinkel, and B. Y. Oh, Phys. Rev. Letters 18 , 630 (1967).
- 11 E. Malamud and P. E. Schlein, Phys. Rev. Letters 19 , 1056 (1967).
- 12 N. N. Biswas, N. M. Cason, P. B. Johnson, V. P. Kenney, J. A. Poirier, W. D. Shephard, and R. Torgerson, Department of Physics, University of Notre Dame preprint (unpublished).
- 13 M. Bander and G. L. Shaw, Phys. Rev. 155 , 1675 (1967); M. Bander, G. L. Shaw, and J. R. Fulco, Phys. Rev. 168 , 1679 (1968).
- 14 M. Bander, University of California, Irvine (private communication to Z. G. T. Guiragossian). We would like to thank Prof. Bander for several illuminating discussions, and for this computation based on our data.

- 15 G. F. Chew and F. E. Low, Phys. Rev. 113 , 1640 (1959);  
C. Goebel, Phys. Rev. Letters 1 , 337 (1958).
- 16 W. Beusch, W. E. Fischer, B. Gobbi, M. Pepin, E. Polgar,  
P. Astbury, G. Brautti, G. Finocchiaro, J. C. Lassalle,  
A. Michelini, K. M. Terwilliger, D. Websdale, and C. H.  
West, Phys. Letters 25B , 357 (1967); T. F. Hoang, D. P.  
Eartly, J. J. Phelan, A. Roberts, C. L. Sandler,  
S. Bernstein, S. Margulies, D. W. McLeod, T. H. Groves,  
N. N. Biswas, N. M. Cason, V. P. Kenney, J. M. Marraffino,  
J. T. McGahan, J. A. Poirier, and W. D. Shephard, to be  
published.
- 17 For P-wave and S-wave amplitudes

$$A_2/A_0 = \frac{6 \sin^2 \delta_1^1}{4/9 \sin^2 \delta_0^0 + 3 \sin^2 \delta_1^1}$$

If  $\delta_0^0 = \pi/2$  when  $\delta_1^1 = \pi/2$ , then  $A_2/A_0 = 1.74$ .

- 18 W. L. Yen, R. L. Eisner, L. Gutay, P. B. Johnson, P. R.  
Klein, R. E. Peters, R. J. Sahni, and G. W. Tautfest, Phys.  
Rev. Letters 18 , 1091 (1967); I. Derado, J. A. Poirier, N. N.  
Biswas, N. M. Cason, V. P. Kenney, and W. D. Shephard,  
Phys. Letters 24B , 112 (1967)..

Table I.

Fit Function	$\ln(\text{LF})$	$\Gamma$	F	$A_1$	$M_1$	$\Gamma_1$	$\frac{P}{\text{TOT}}$	$A_2$	$M_2$	$\Gamma_2$
1 (M)	- 3.26	const	1.0	.467	.776	.152	.368	.168	1.266	.195
2 ( $M^2$ )	-17.06	const	1.0	.522	.780	.142	.340	.586	1.266	.216
3 ( $M^2$ )	- 9.08	const	$F_1$	.543	.776	.148	.382	.748	1.264	.210
4 ( $M^2$ )	.0	$\Gamma_1$	$F_1$	.555 $\pm .021$	.775 $\pm .002$	.154 $\pm .006$	.404 $\pm .015$	.618 $\pm .04$	1.268 $\pm .006$	.176 $\pm .013$
5 ( $M^2$ )	- 2.03	$\Gamma_2$	$F_1$	.548	.776	.152	.394	.673	1.266	.191
average				.527 $\pm .033$	.777 $\pm .002$	.150 $\pm .004$	.377 $\pm .022$	.656 $\pm .04$	1.266 $\pm .006$	.197 $\pm .013$

Fit function no. 1 is Eqs. (3) and (5); fit functions nos. 2 through 5 are Eqs. (4) and (5) (mass-squared)

fit).  $F_1 = (M/M_0) (Q_0/Q)$ , where  $Q^2 = (M/2)^2 - m^2$ ,  $Q_0^2 = (M_0/2)^2 - m^2$ .  $\Gamma_1 = \Gamma_0 (Q/Q_0)^3 D/D_0$  where

$D = 1.0 + (Q/0.777)^2$  and  $\Gamma_2 = \Gamma_0 (Q/Q_0)^3 (M_0/M)$ . Of the fits tried, fit no. 4 is the best fit in terms of

$\ln(\text{LF})$ .

FIGURE CAPTIONS

- Fig. 1 The  $\pi^+\pi^-$  effective mass spectrum for events with  $\cos \theta_{pn}^* < 0.0$  (full histogram),  $\cos \theta_{pn}^* < -0.6$  (shaded histogram).
- Fig. 2 Number of events in the  $\rho^0$  band (0.70  $\rightarrow$  0.85 GeV) as a function of  $\cos \theta_{pn}^*$ , the cosine of the center of mass scattering angle.
- Fig. 3 The  $\pi^+\pi^-$  decay angular distribution in the  $\rho$  band (0.70  $\rightarrow$  0.85 GeV) for three intervals in the center of mass angle  $\theta_{pn}^*$ .
- Fig. 4 Decay angular distributions for events in the  $\rho^0$  band (0.70  $\rightarrow$  0.85 GeV) with  $\cos \theta_{pn}^* < -0.6$ .
- Fig. 5 The  $\pi^0\pi^-$  effective mass spectrum for events with  $\cos \theta_{pp}^* < -0.6$ .
- Fig. 6 Number of events in the  $\rho^-$  band (0.70  $\rightarrow$  0.85 GeV) as a function of  $\cos \theta_{pp}^*$ , the cosine of the center of mass scattering angle.
- Fig. 7 The  $n\pi^-$  effective mass spectrum. All events for which the  $\pi^+\pi^-$  effective mass is in the  $\rho$  band (0.70  $\rightarrow$  0.85 GeV) have been excluded. (a)  $\cos \theta_{\pi^-\pi^+}^* < -0.6$ . The shaded events are those for which  $\cos \theta_{\pi^-\pi^+}^* > 0.9$ . (b)  $-0.6 < \cos \theta_{\pi^-\pi^+}^* < 0.0$ .

- Fig. 8 The  $\pi\pi^-$  effective mass spectrum for events with  $\cos \theta_{\pi^-\pi^0}^* < -0.6$ . All events for which the  $\pi^0\pi^-$  effective mass is in the  $\rho$  band (0.70 → 0.85 GeV) have been excluded.
- Fig. 9 The  $n\pi^+$  effective mass spectrum for events with  $\cos \theta_{n\pi^-}^* < -0.6$ . All events for which the  $\pi^+\pi^-$  effective mass is in the  $\rho$  band (0.70 → 0.85 GeV) have been excluded.
- Fig. 10 The  $\pi\pi^0$  effective mass spectrum for events with  $\cos \theta_{p\pi^-}^* < -0.6$ . All events for which the  $\pi^0\pi^-$  effective mass is in the  $\rho$  band (0.70 → 0.85 GeV) have been excluded.
- Fig. 11 The  $\pi^+\pi^-$  effective mass spectrum. The shaded events are those with  $\cos \theta_{pn}^* \geq 0.94$ . The fitted curve is obtained assuming constant width resonances and phase space.
- Fig. 12 Dalitz plots for the reaction  $\pi^-p \rightarrow \pi^0\pi^-p$ .  
 (a)  $n\pi^-$  effective mass squared vs.  $\pi^+\pi^-$  effective mass squared. (b)  $n\pi^-$  effective mass squared vs.  $n\pi^+$  effective mass squared.
- Fig. 13 Scatter plot of  $\sqrt{-t/\mu^2}$  vs. the  $\pi^+\pi^-$  effective mass.
- Fig. 14 Scatter plot of  $\cos \theta_{\pi^-\pi^-}$  vs. the  $\pi^+\pi^-$  effective mass.

- Fig. 15  $d\sigma/dt$  for  $\rho^0$  production normalized to a total  $\rho^0$  cross section of 1.15 mb.
- Fig. 16  $\cos \theta_{\pi^+\pi^-}$  vs.  $\phi$  for  $\pi^+\pi^-$  effective mass in the  $\rho^0$  band (0.75  $\rightarrow$  0.85 GeV) and  $|t| < 0.2$  (GeV/c)<sup>2</sup>.
- Fig. 17 The  $t$  dependence of the density-matrix elements for events in the  $\rho^0$  band (0.70  $\rightarrow$  0.85 GeV). The curves are taken from an absorption model calculation which includes S-P-wave interference (Ref. 4).
- Fig. 18 The  $t$  dependence of the S-P-wave interference density-matrix elements for events in the  $\rho^0$  band (0.70  $\rightarrow$  0.85 GeV). The curves are taken from Ref. 4.
- Fig. 19 The  $t$  dependence of the density-matrix elements in the  $\rho$  helicity frame for events in the  $\rho^0$  band (0.70  $\rightarrow$  0.85 GeV).
- Fig. 20 The  $t$  dependence of the S-P-wave interference density-matrix elements for events in the  $\rho^0$  band (0.70  $\rightarrow$  0.85 GeV).
- Fig. 21 Forward backward asymmetry  $g$  as a function of  $\pi^+\pi^-$  effective mass for  $|t| < 0.2$  (GeV/c)<sup>2</sup>.
- Fig. 22 The  $I = 0$ , S-wave  $\pi\pi$  phase shift as a function of the dipion effective mass. The various results are taken from the following references:

J. P. Baton and J. Reignier, *Nuovo Cimento* 36,  
1149 (1965); L. W. Jones, D. O. Caldwell,  
B. Zacharov, D. Harting, E. Bleuler, W. C.  
Middlekoop, and B. Elsner, *Phys. Letters* 21, 590  
(1966), and Refs. 4, 7, 10, 11, and 12 in the text.

Fig. 23 The  $\delta_0^0$ ,  $\delta_0^2$ ,  $\delta_1^1$   $\pi\pi$  phase shifts as functions of  
the dipion effective mass.  $\delta_0^0$  is calculated from  
scattering length parameters suggested by Bander  
(see text).  $\delta_0^2$  is taken from Ref. 9.

Fig. 24 The forward-backward asymmetry as a function of  
 $\pi^+\pi^-$  effective mass for  $|t| < 3\mu^2$  and for  $3\mu^2 <$   
 $|t| < 10\mu^2$ . The curves are calculated from the  
phase shifts in Fig. 23 and the model in Ref. 13.

Fig. 25 The elastic  $\pi^+\pi^-$  cross section obtained from an  
extrapolation to the pole as a function of the  $\pi^+\pi^-$   
effective mass. The curves are the unitary limits  
for spin 1 and spin 2 particles.

Fig. 26 Legendre coefficients from fits to the  $\pi^+\pi^-$  decay  
angular distributions for events with  
 $|t| < 0.2 (\text{GeV}/c)^2$ .

Fig. 27 Legendre coefficients from fits to the  $\pi^0\pi^-$  decay  
angular distribution for events with  
 $|t| < 0.4 (\text{GeV}/c)^2$ .

Fig. 28 The  $t$  dependence of  $A_1/A_0$  and  $A_2/A_0$  in the  $\pi^+\pi^-$  decay angular distribution.

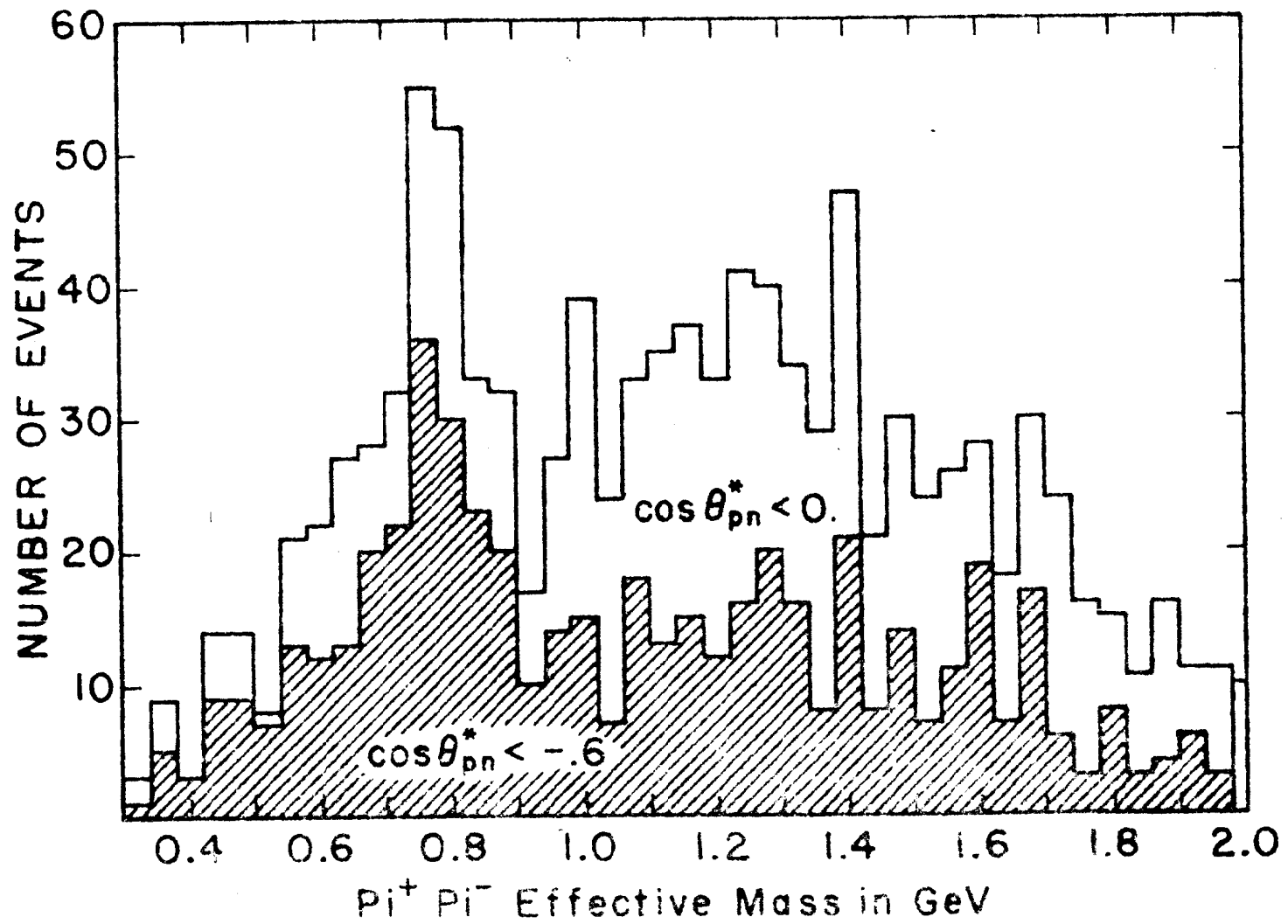


Fig. 1

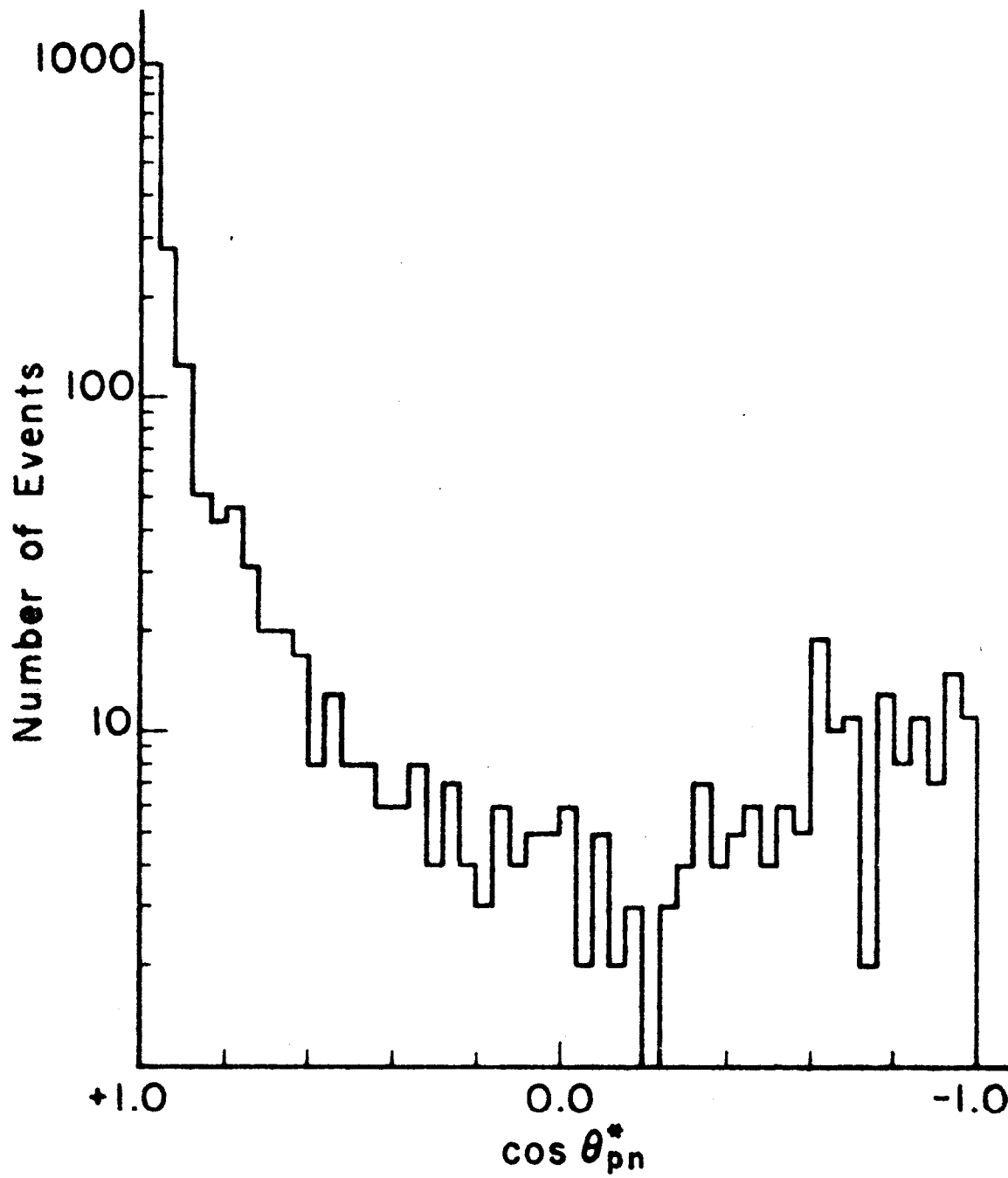


Fig. 2

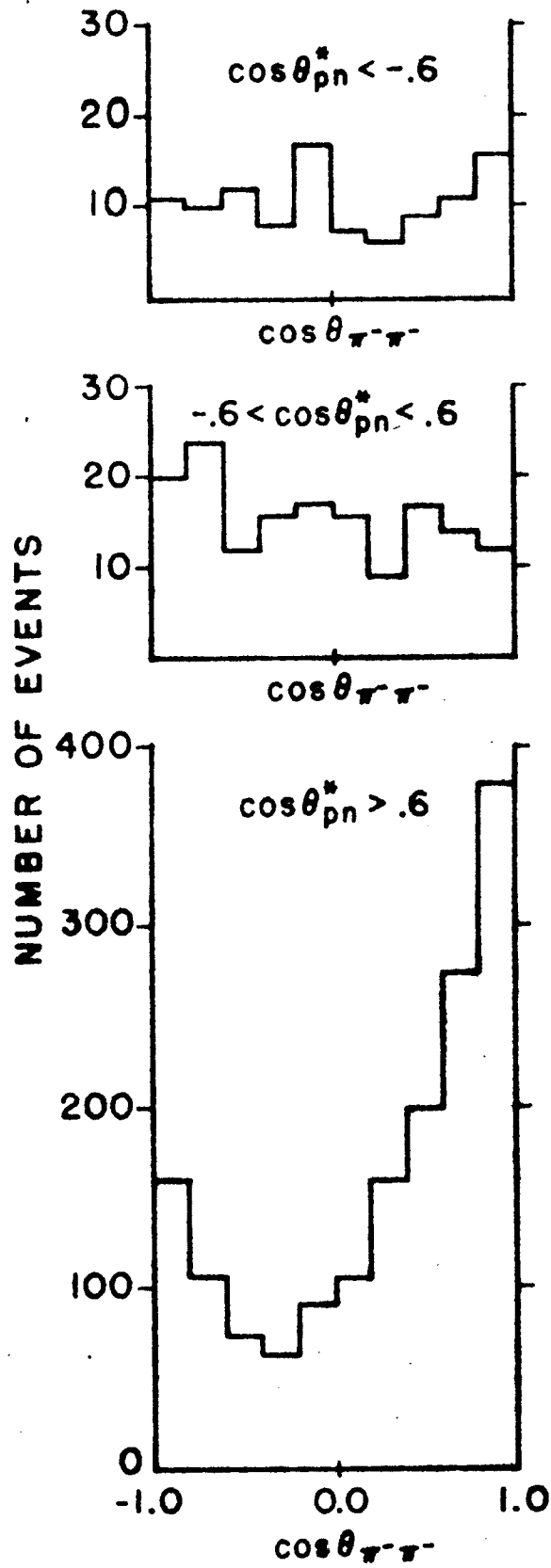


Fig. 3

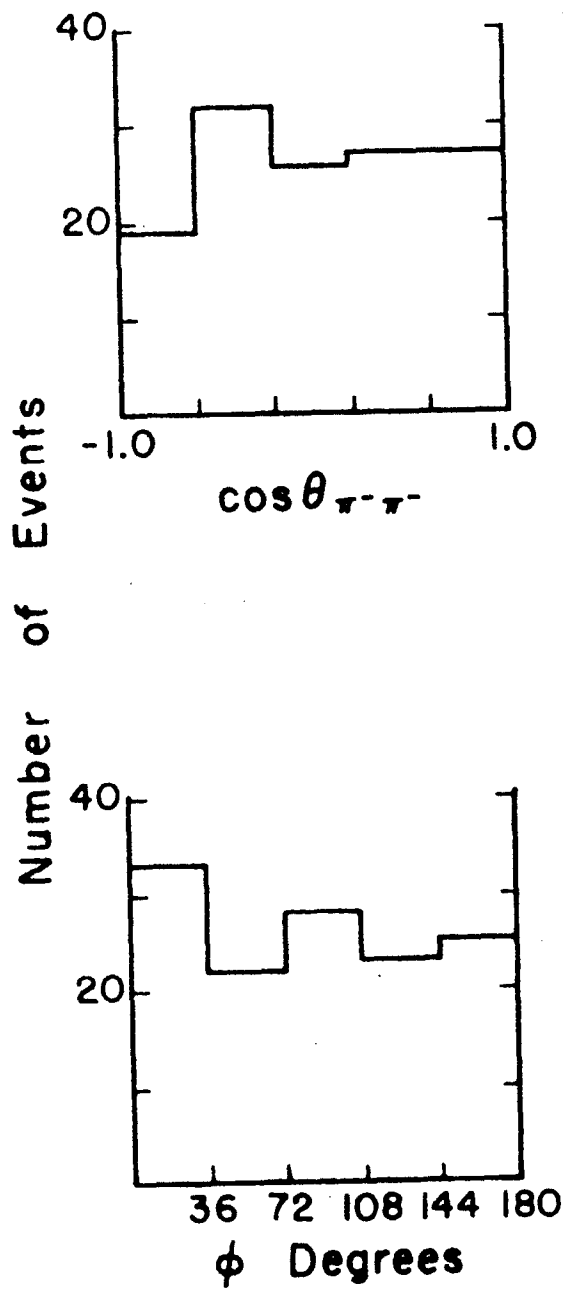


Fig. 4

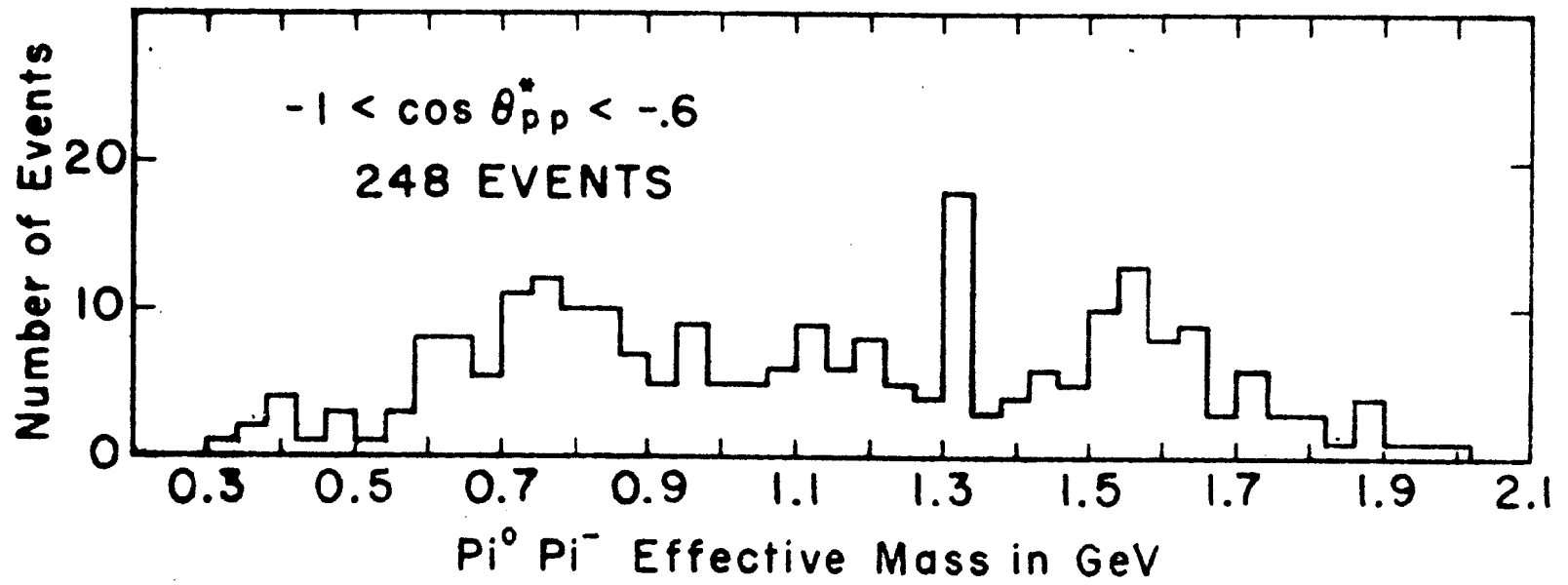


Fig. 5

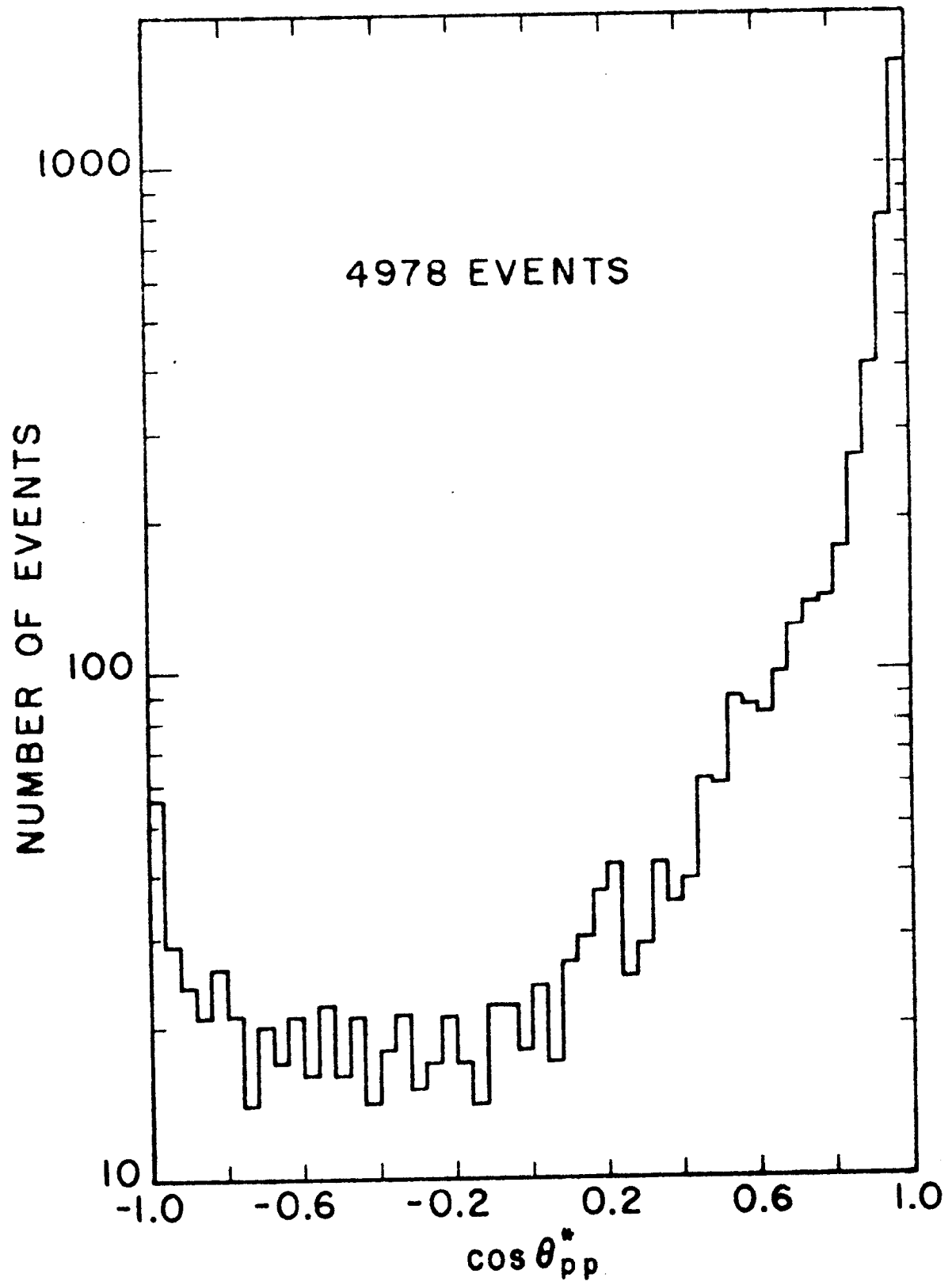


Fig. 6

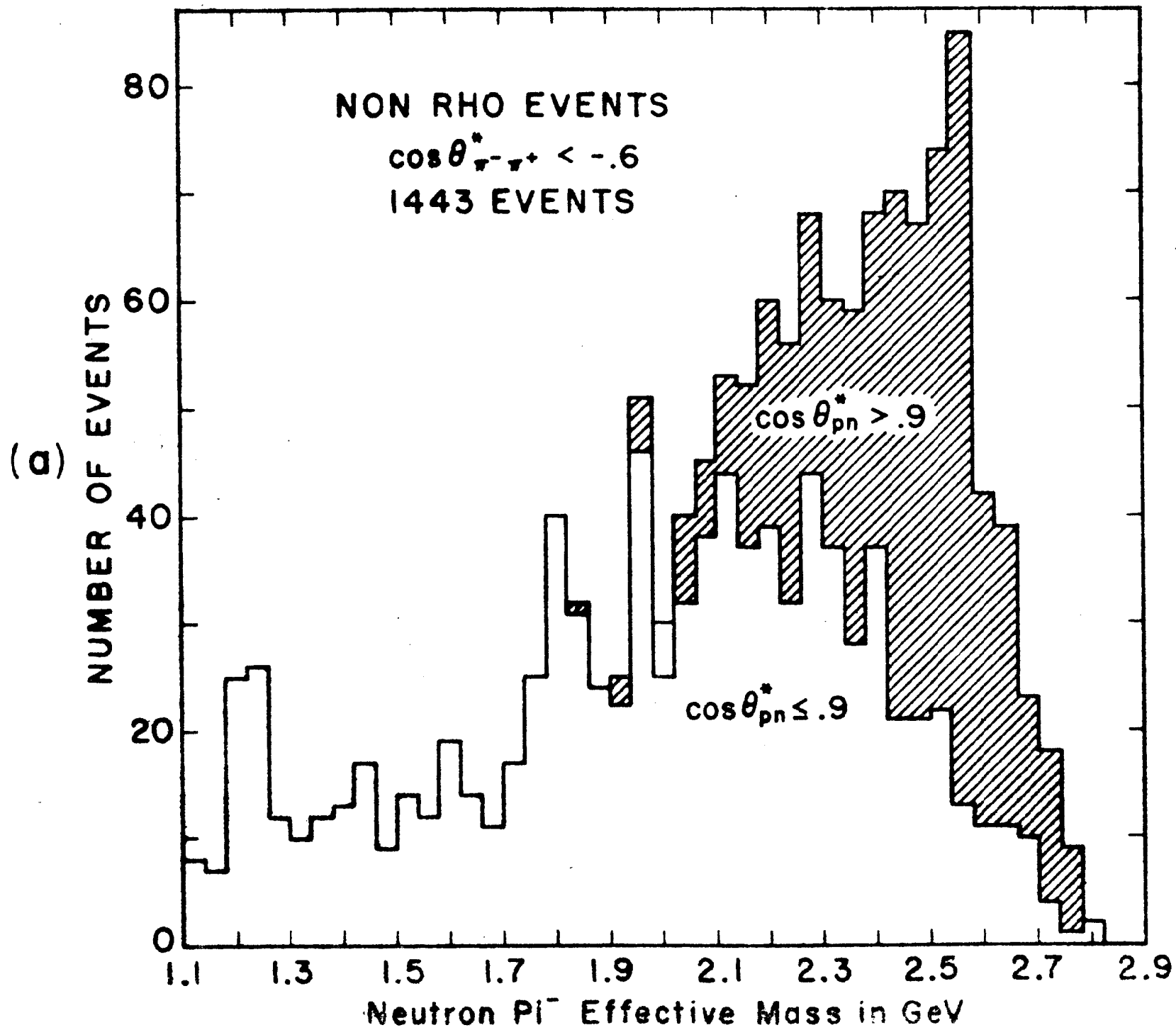


Fig. 7a

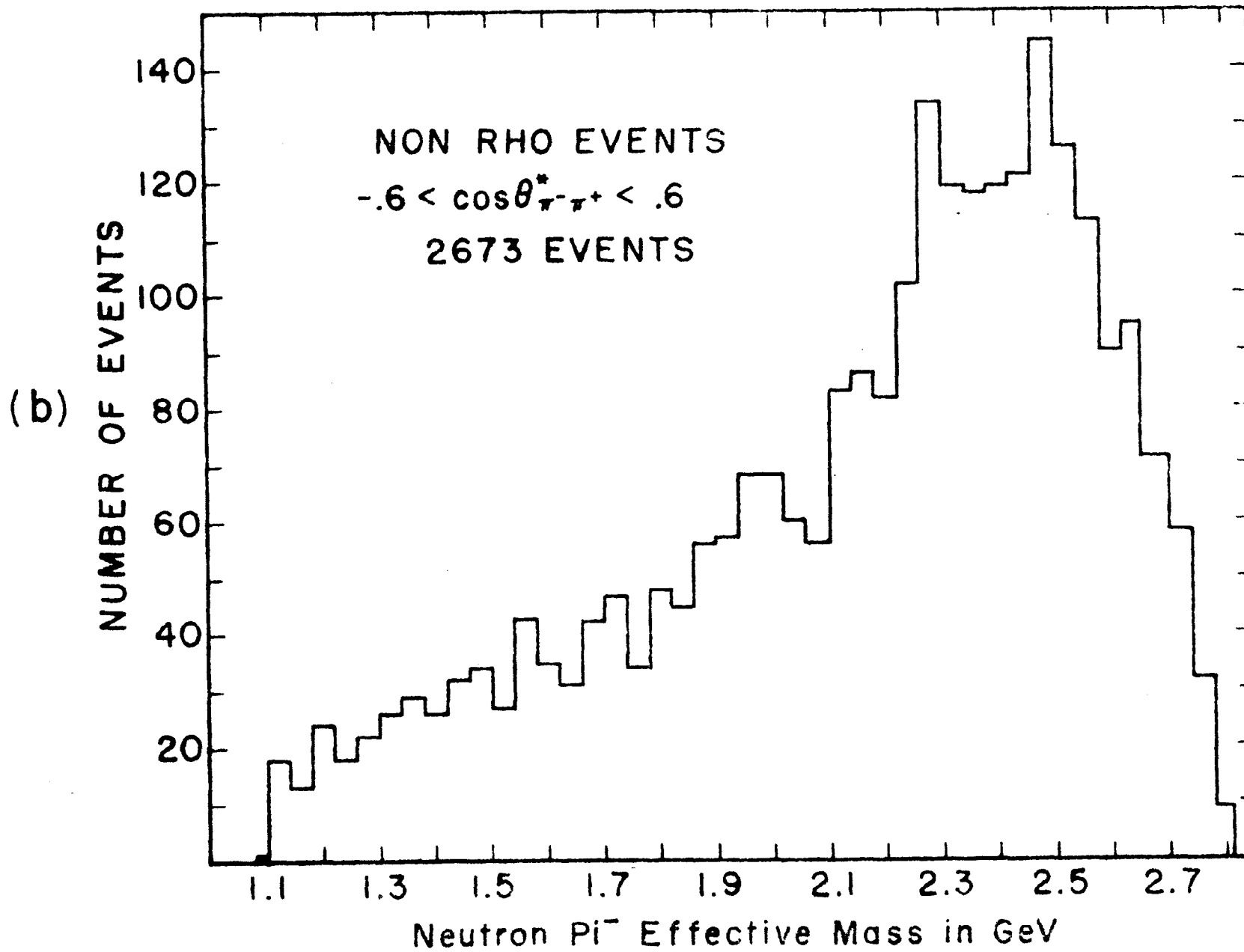


Fig. 7b

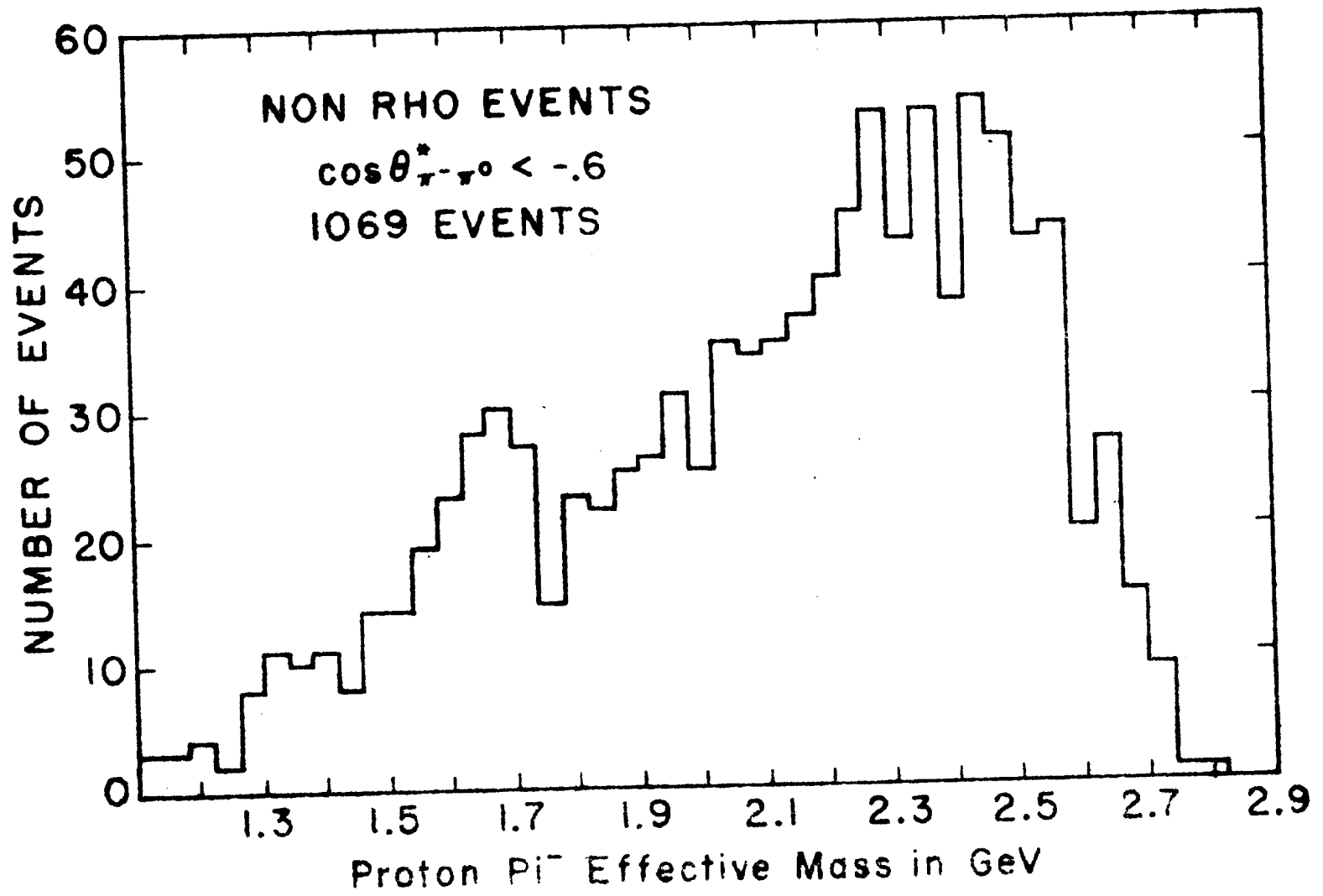


Fig. 8

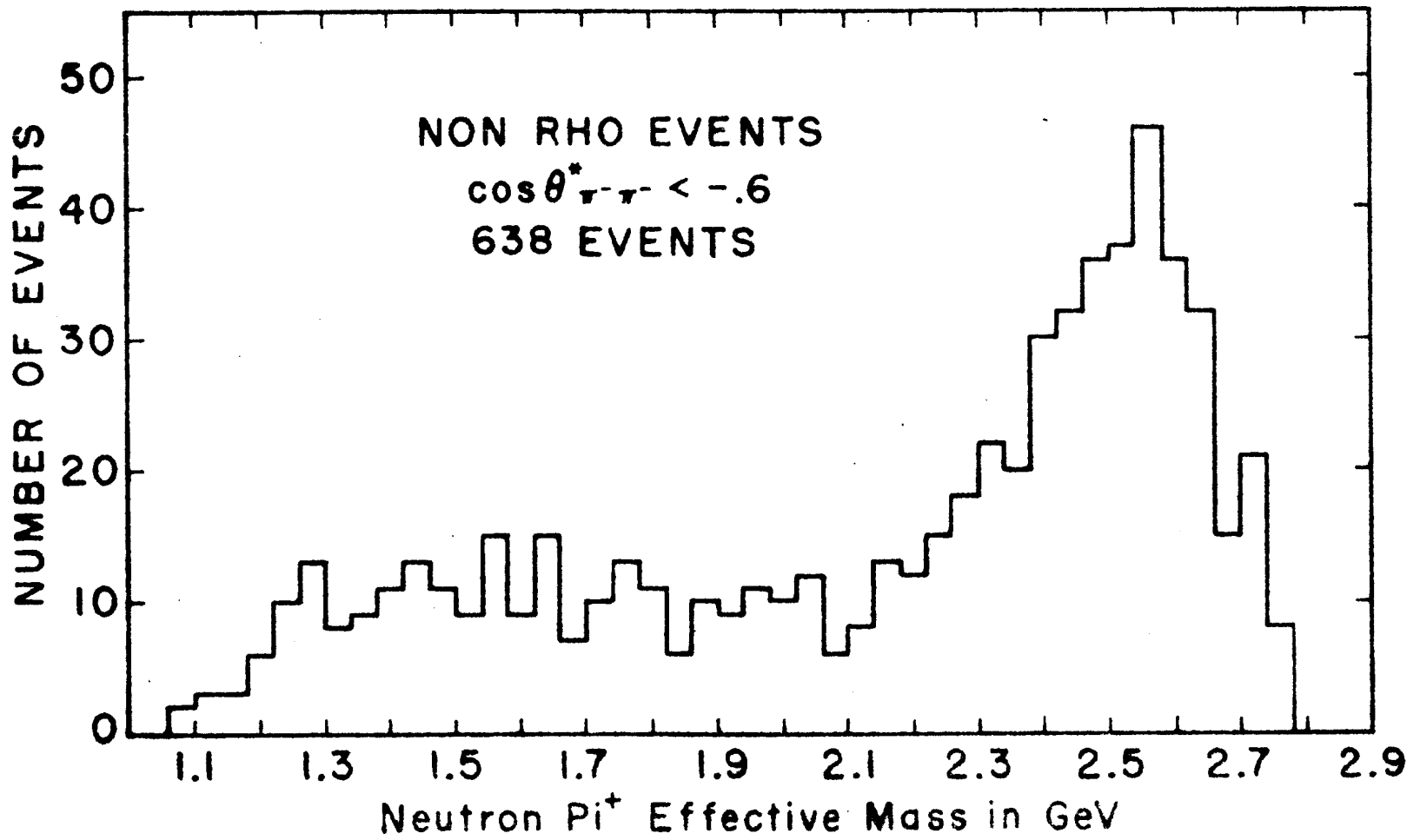


Fig. 9

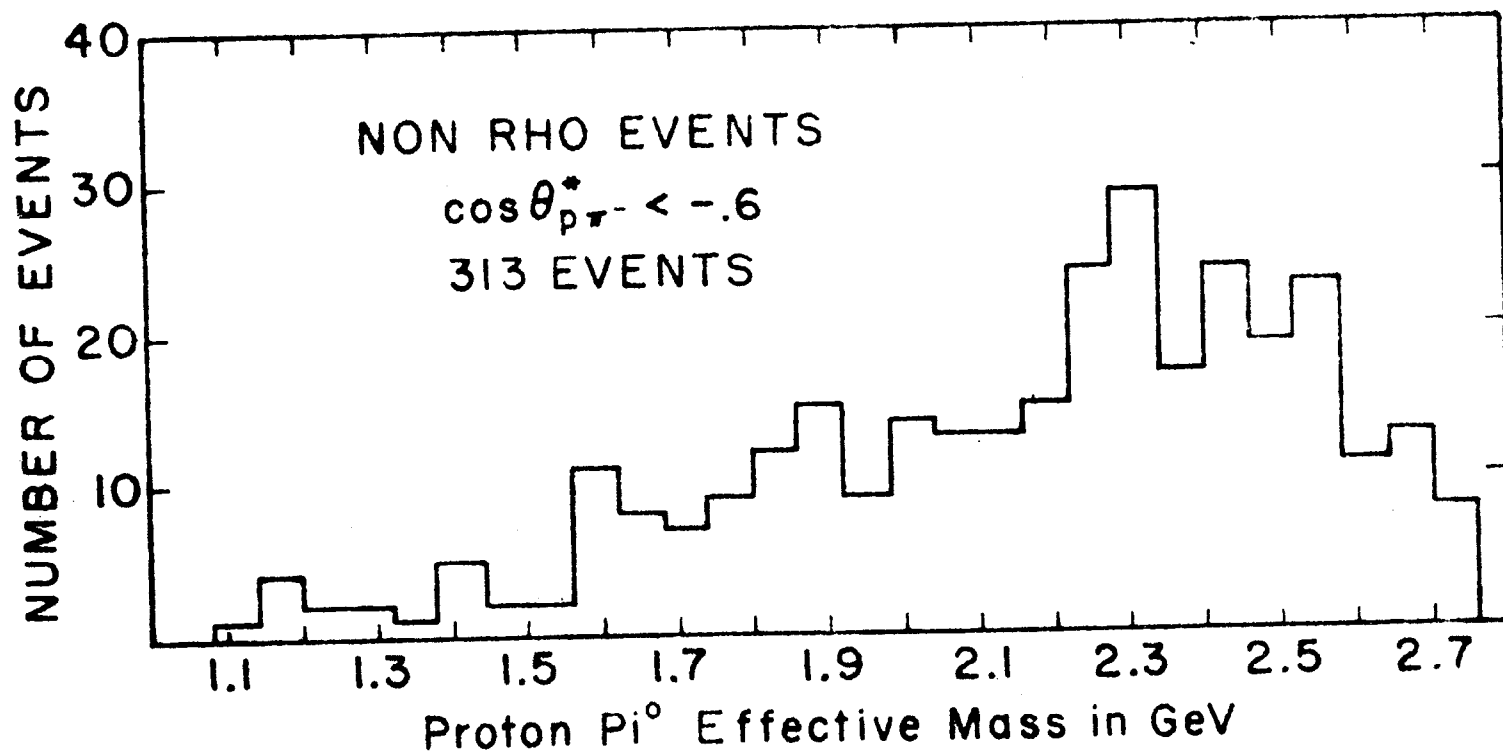
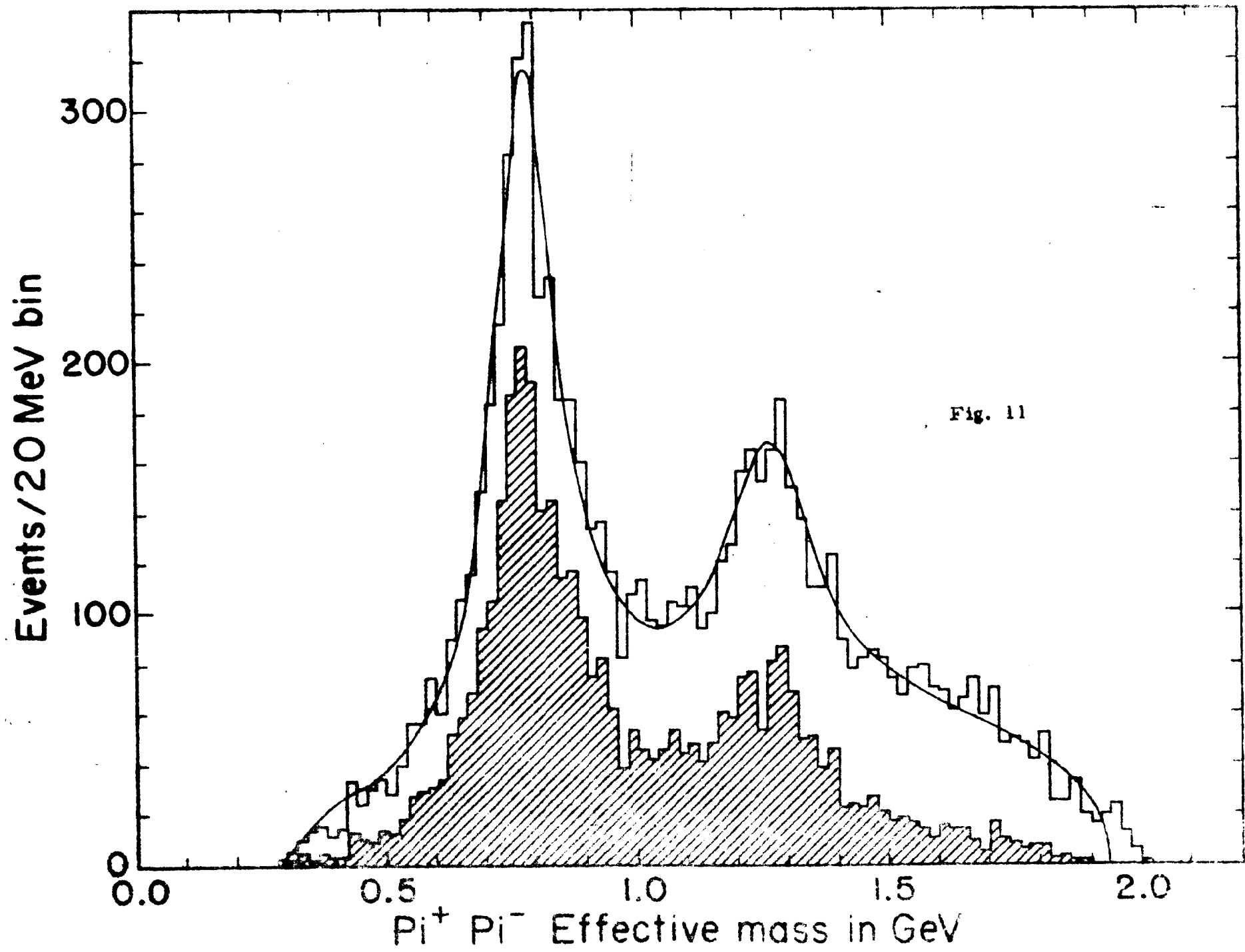


Fig. 10



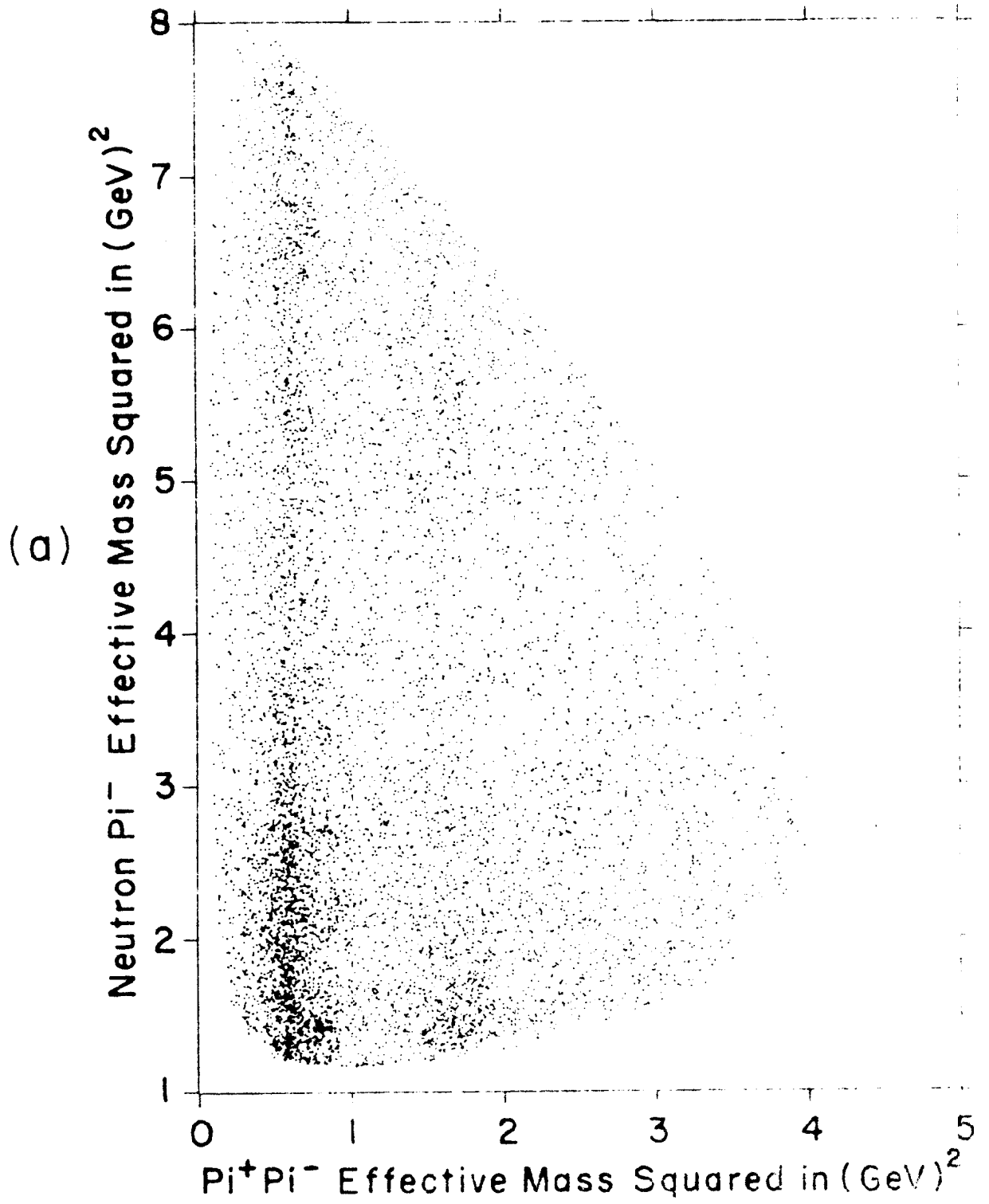


Fig. 124

(b)

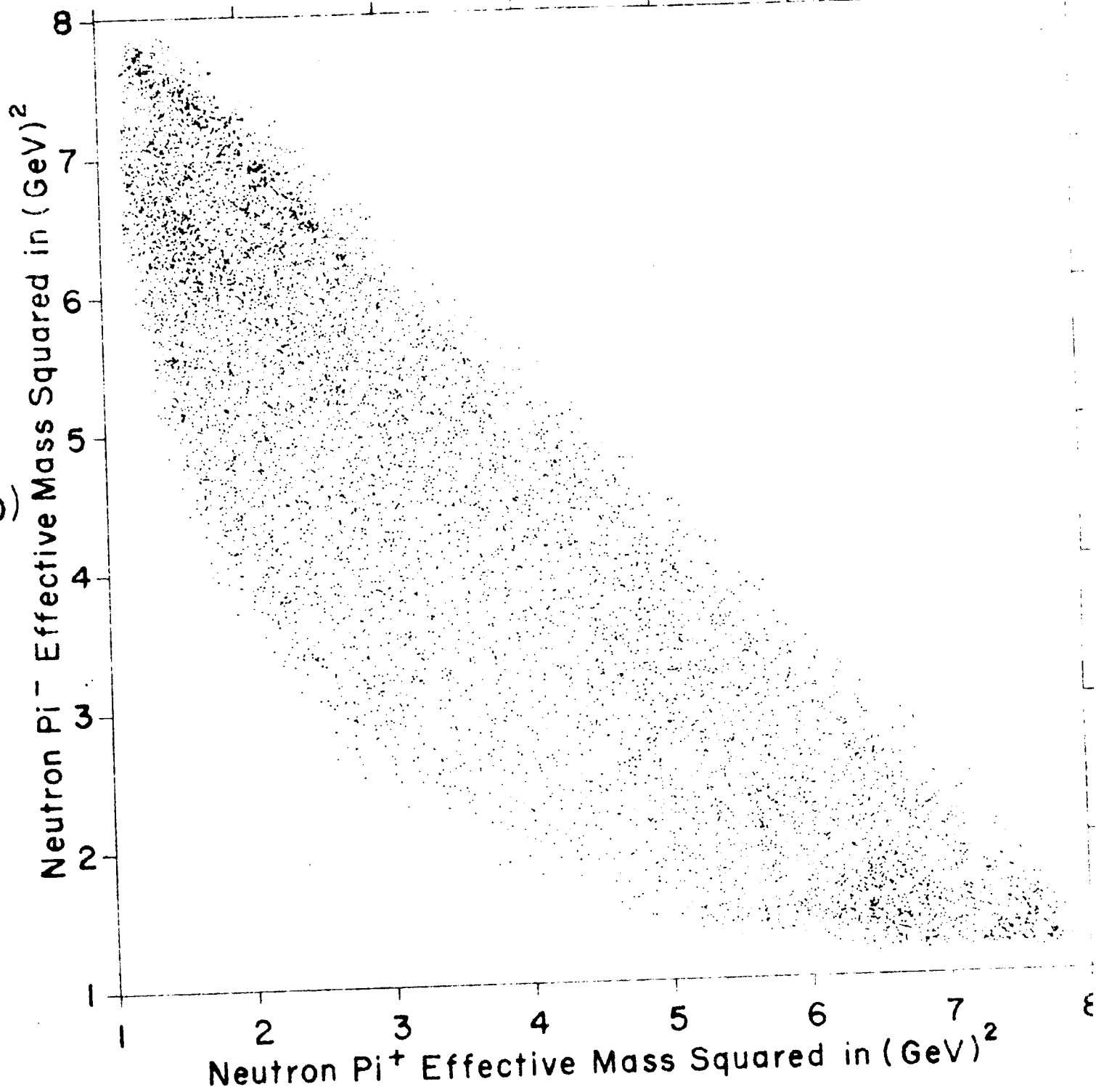


Fig. 12b

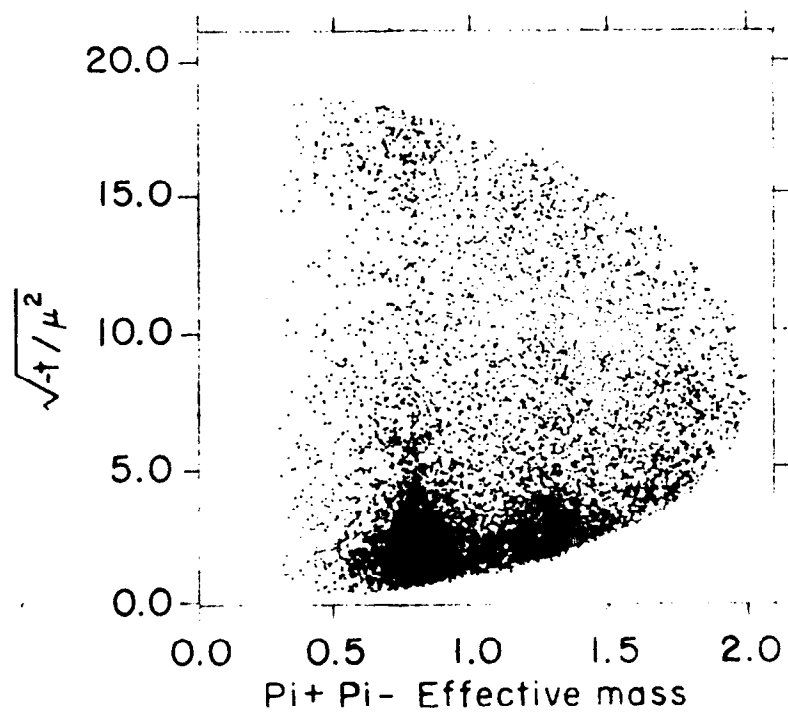


Fig. 13

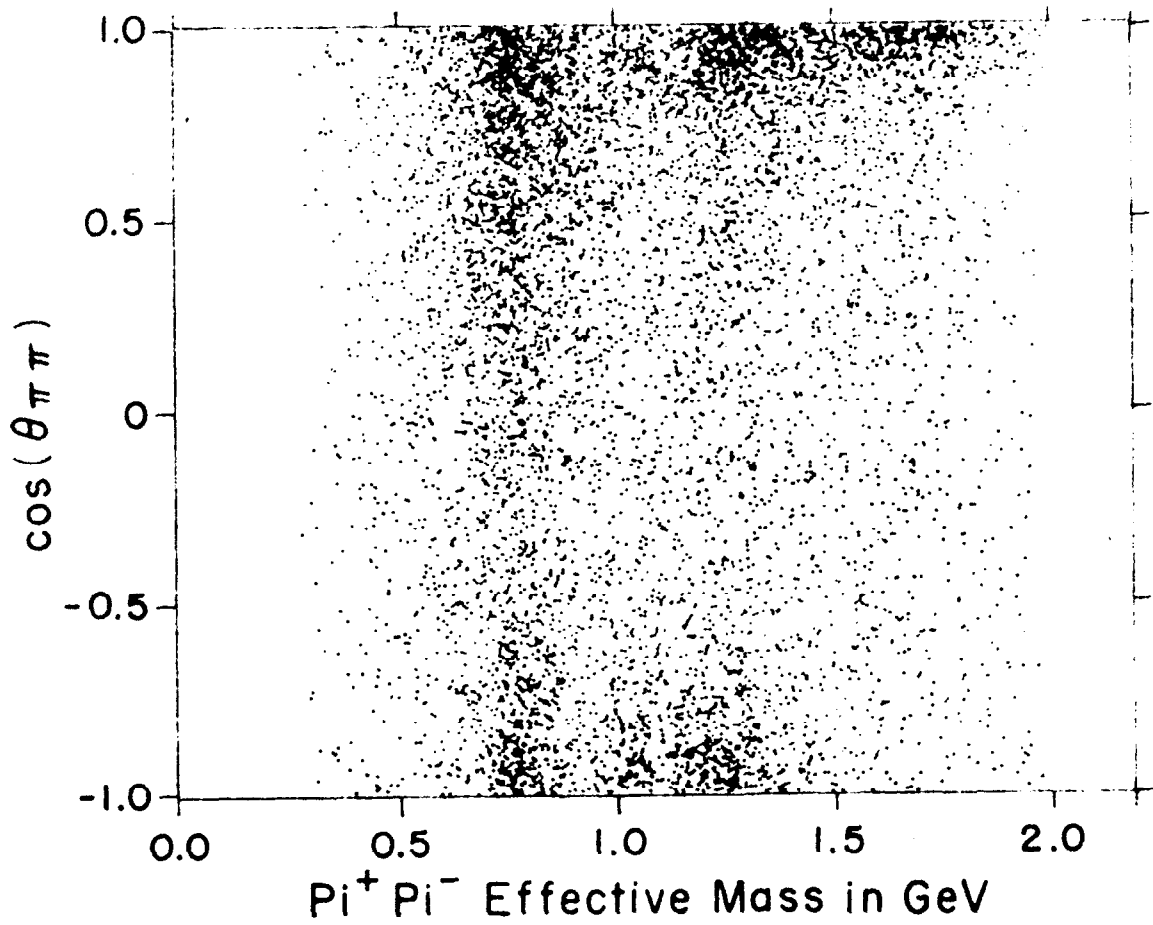
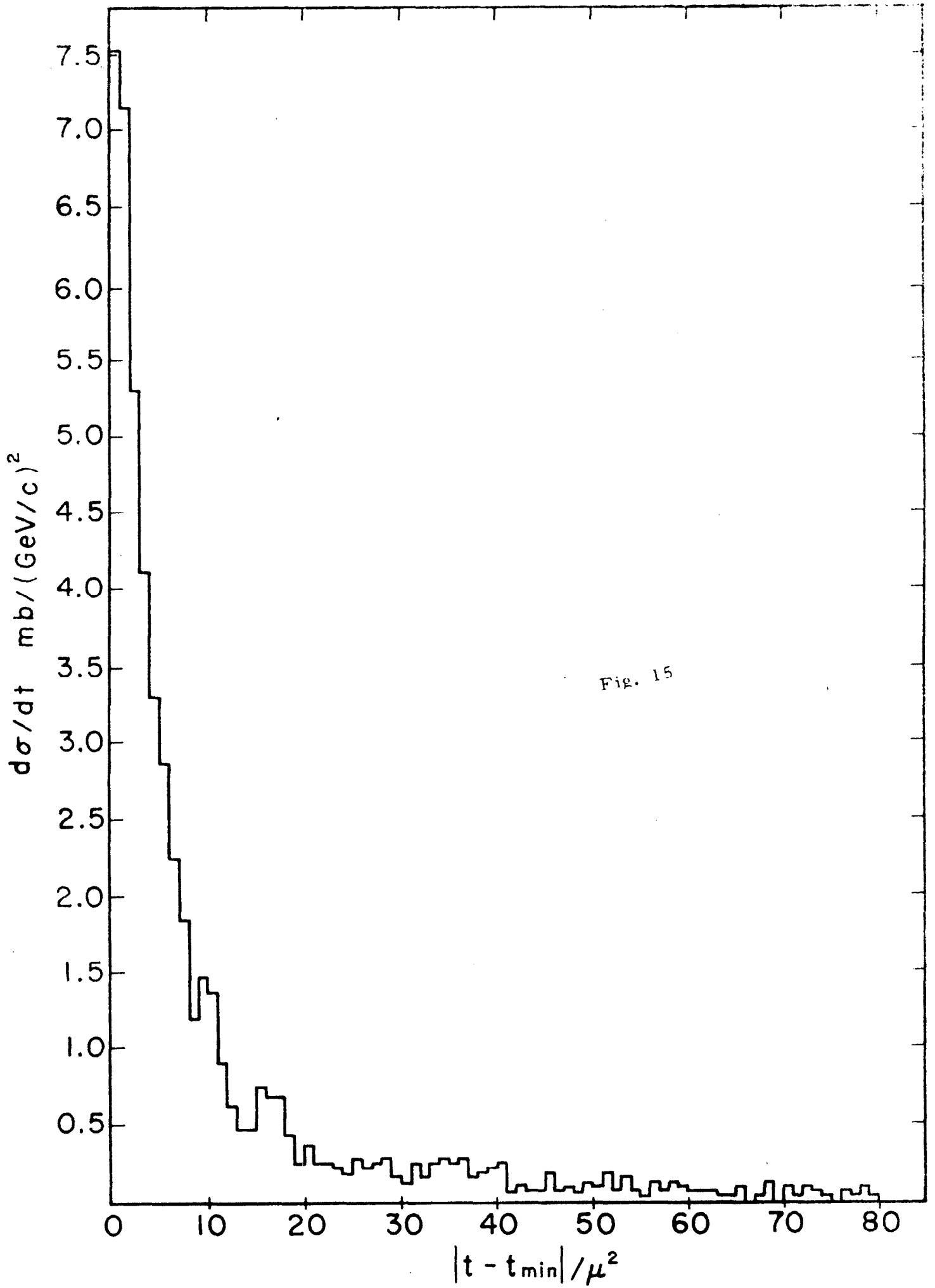


Fig. 14



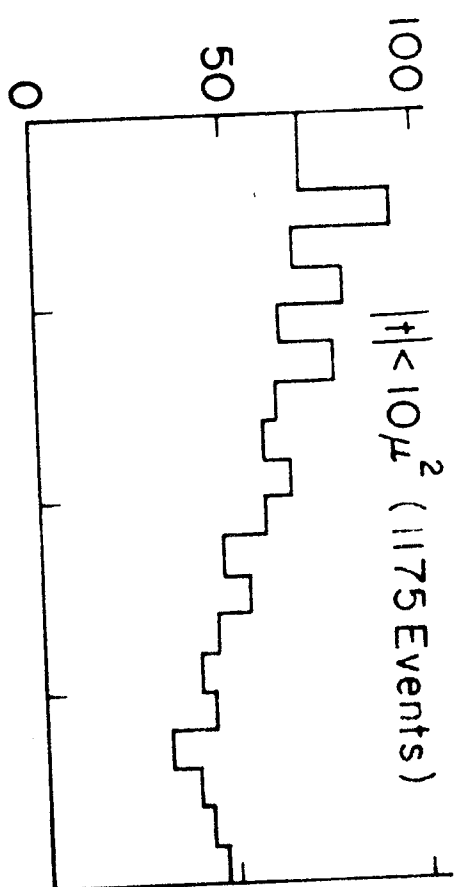
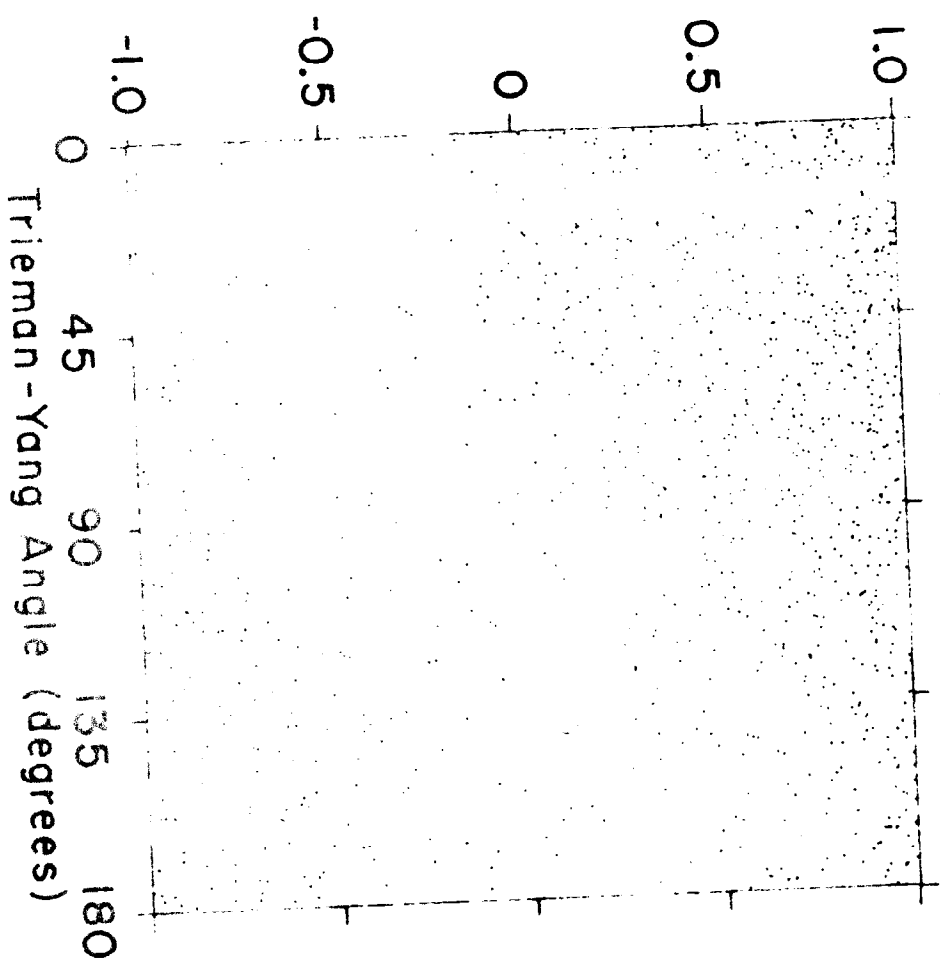
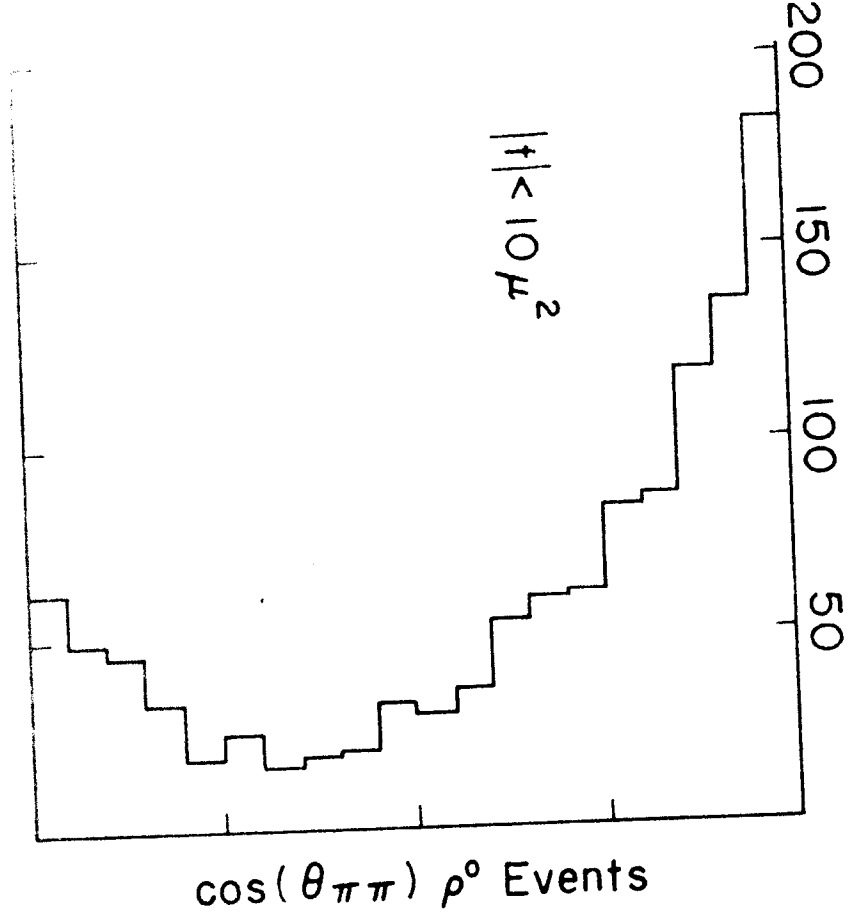


Fig. 1c



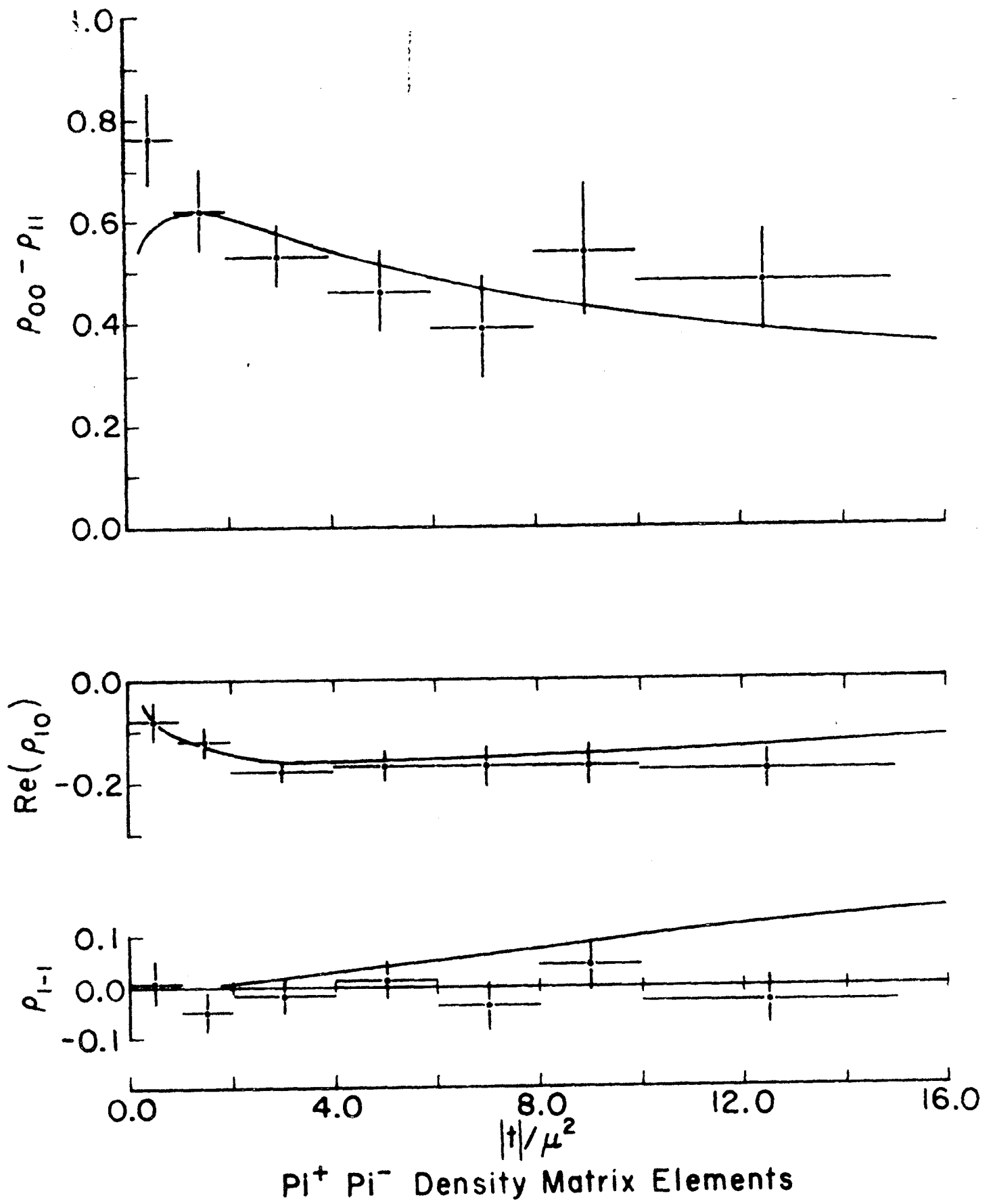


Fig. 17

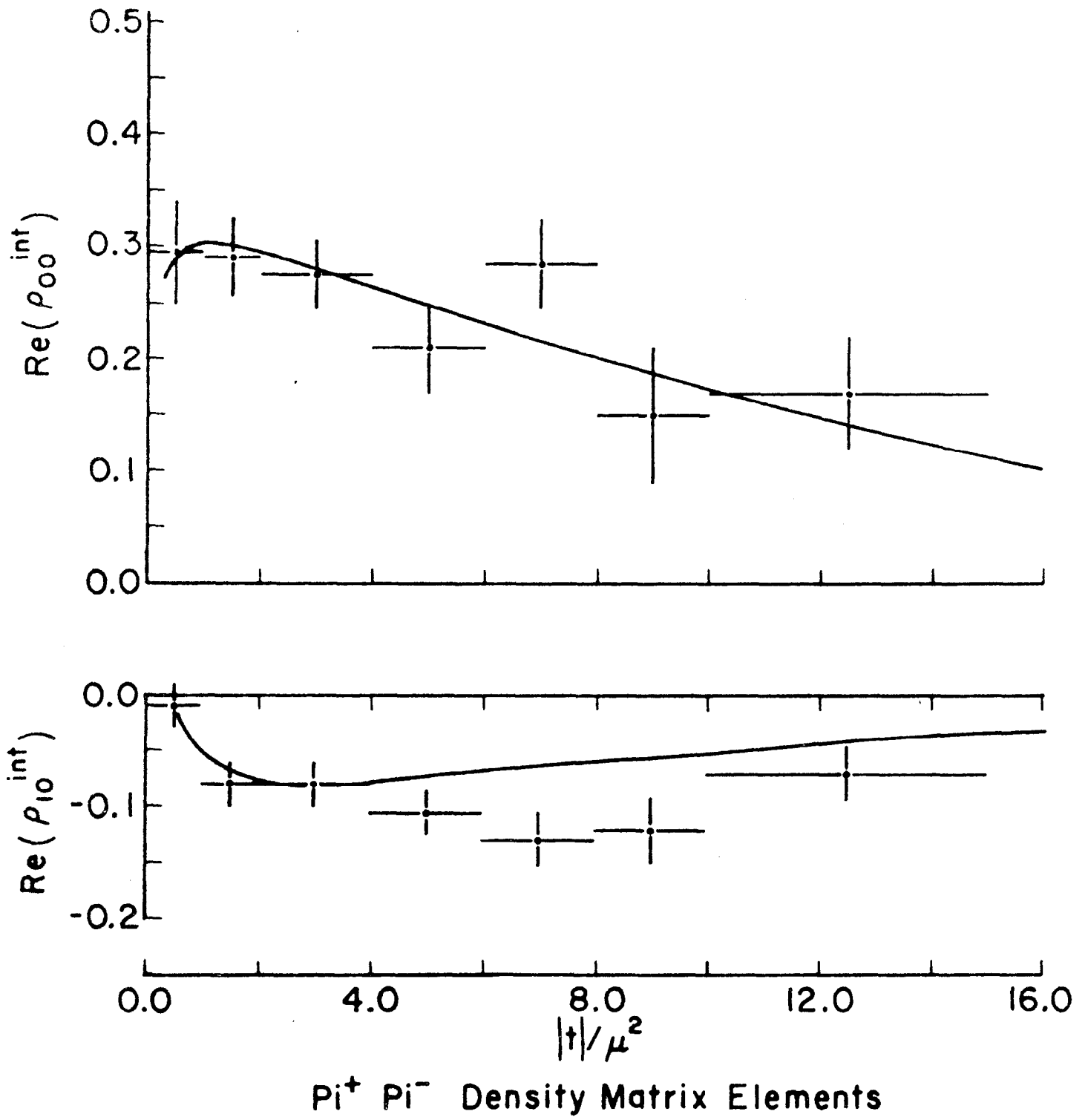


Fig. 18

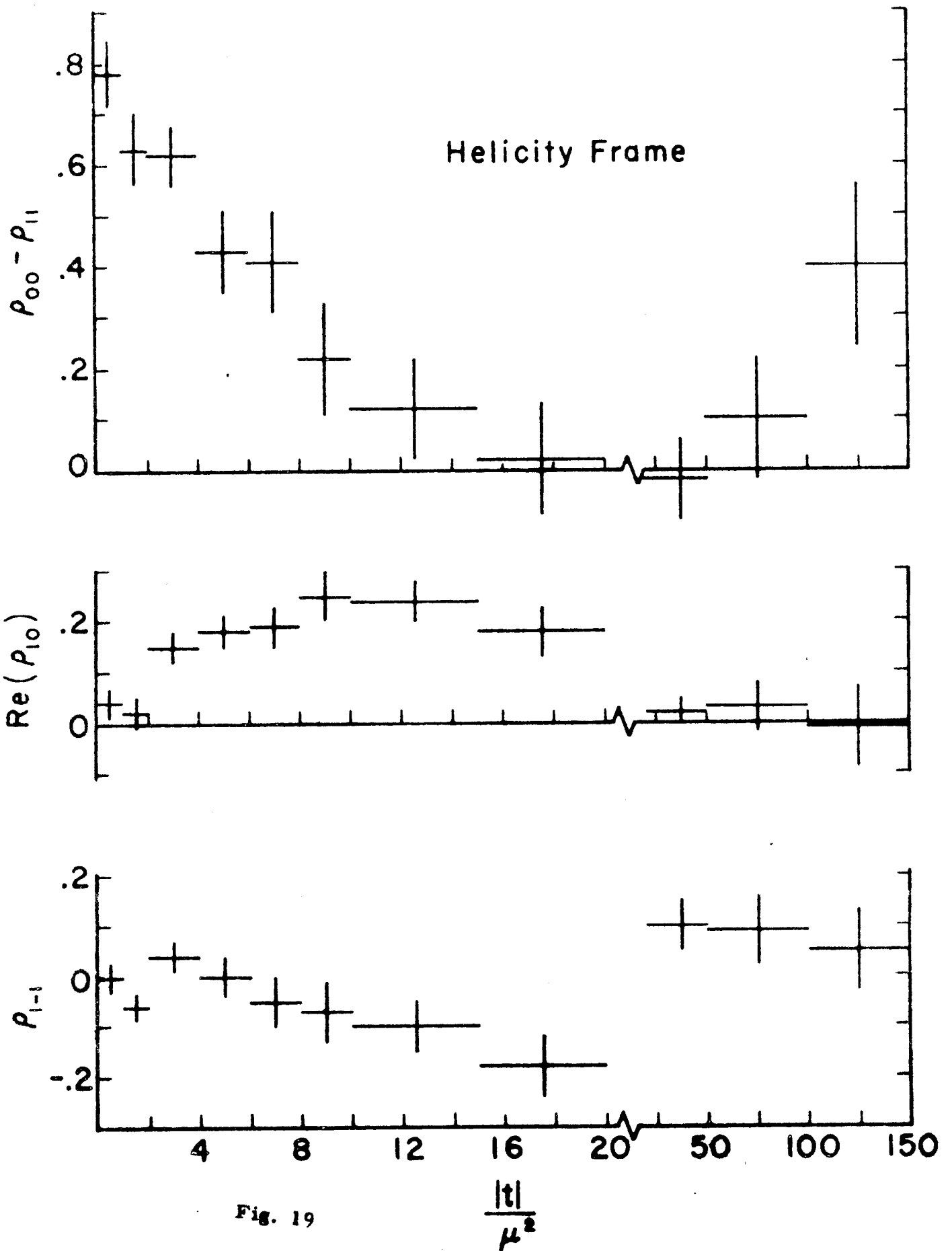


Fig. 19

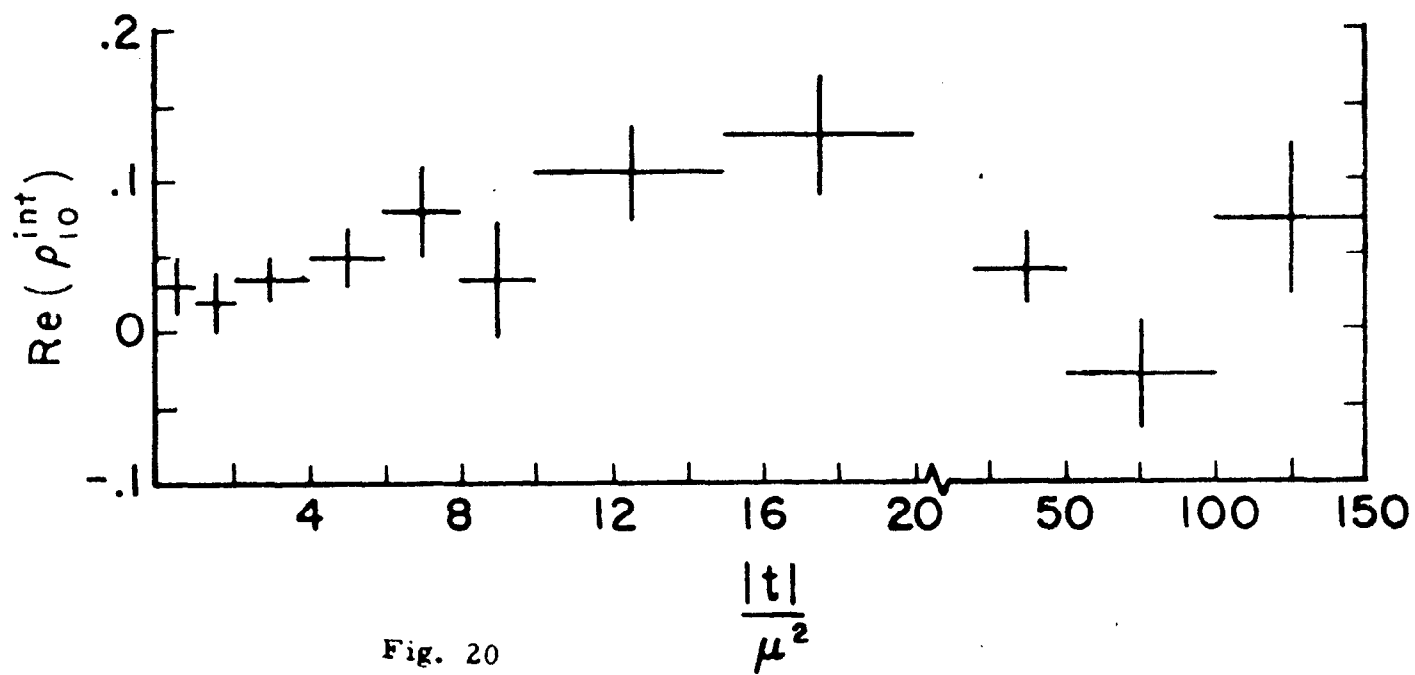
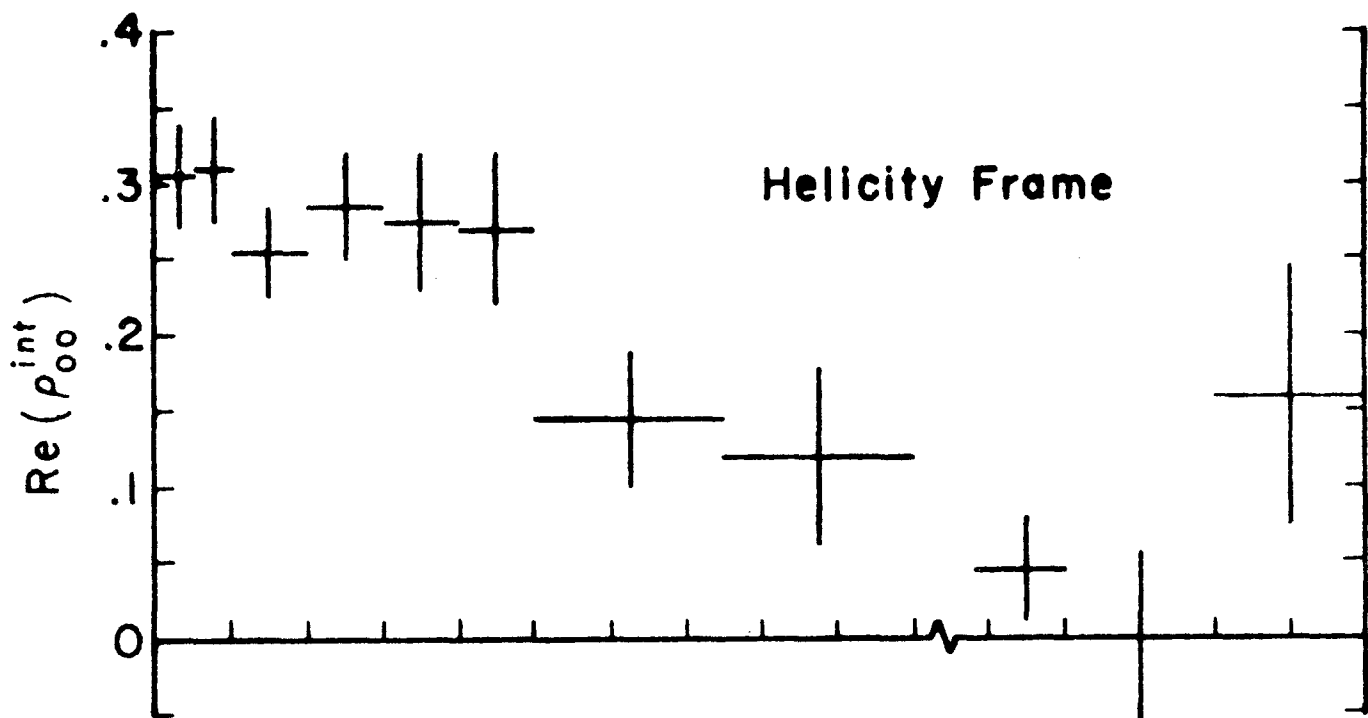
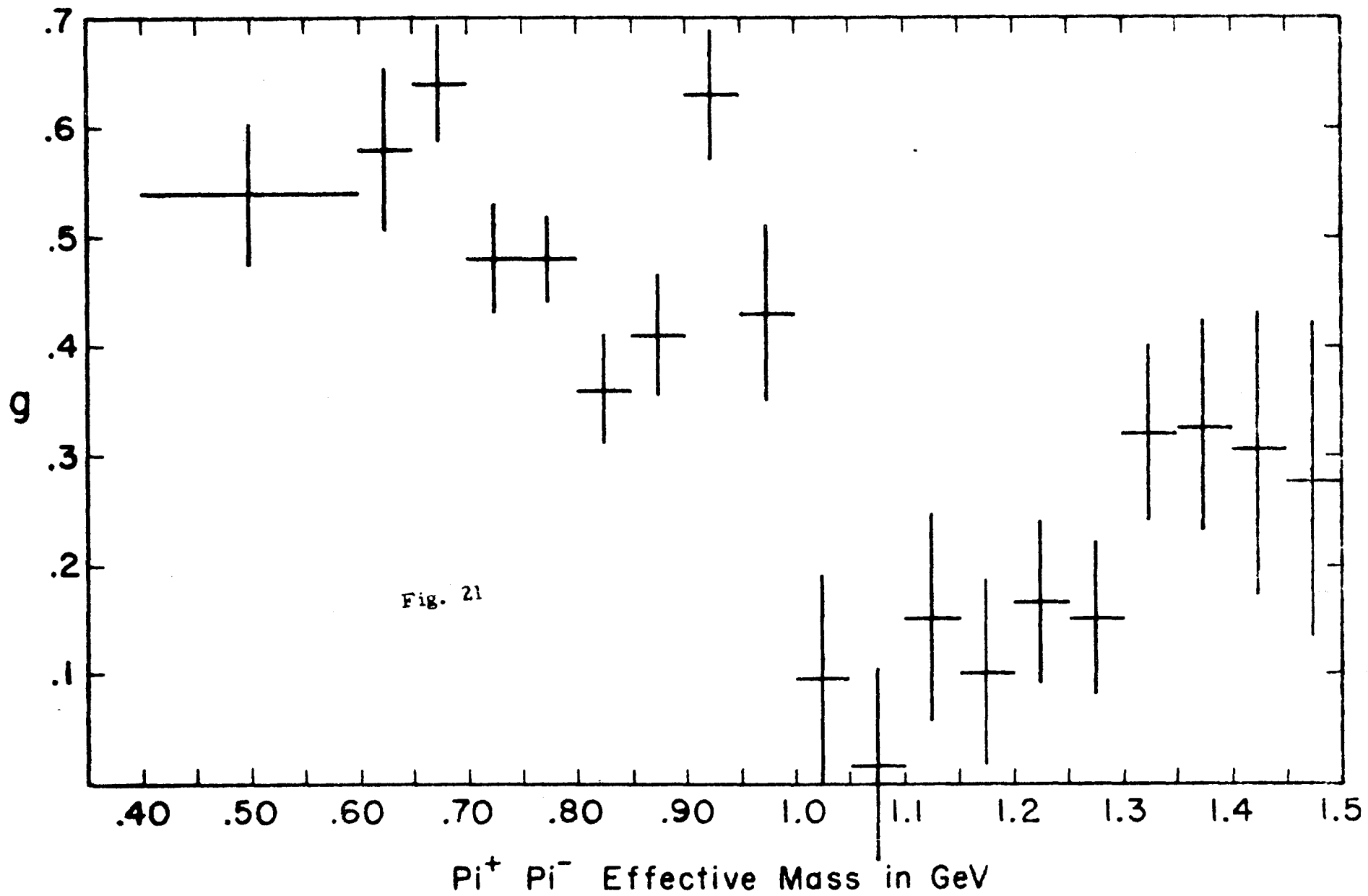


Fig. 20



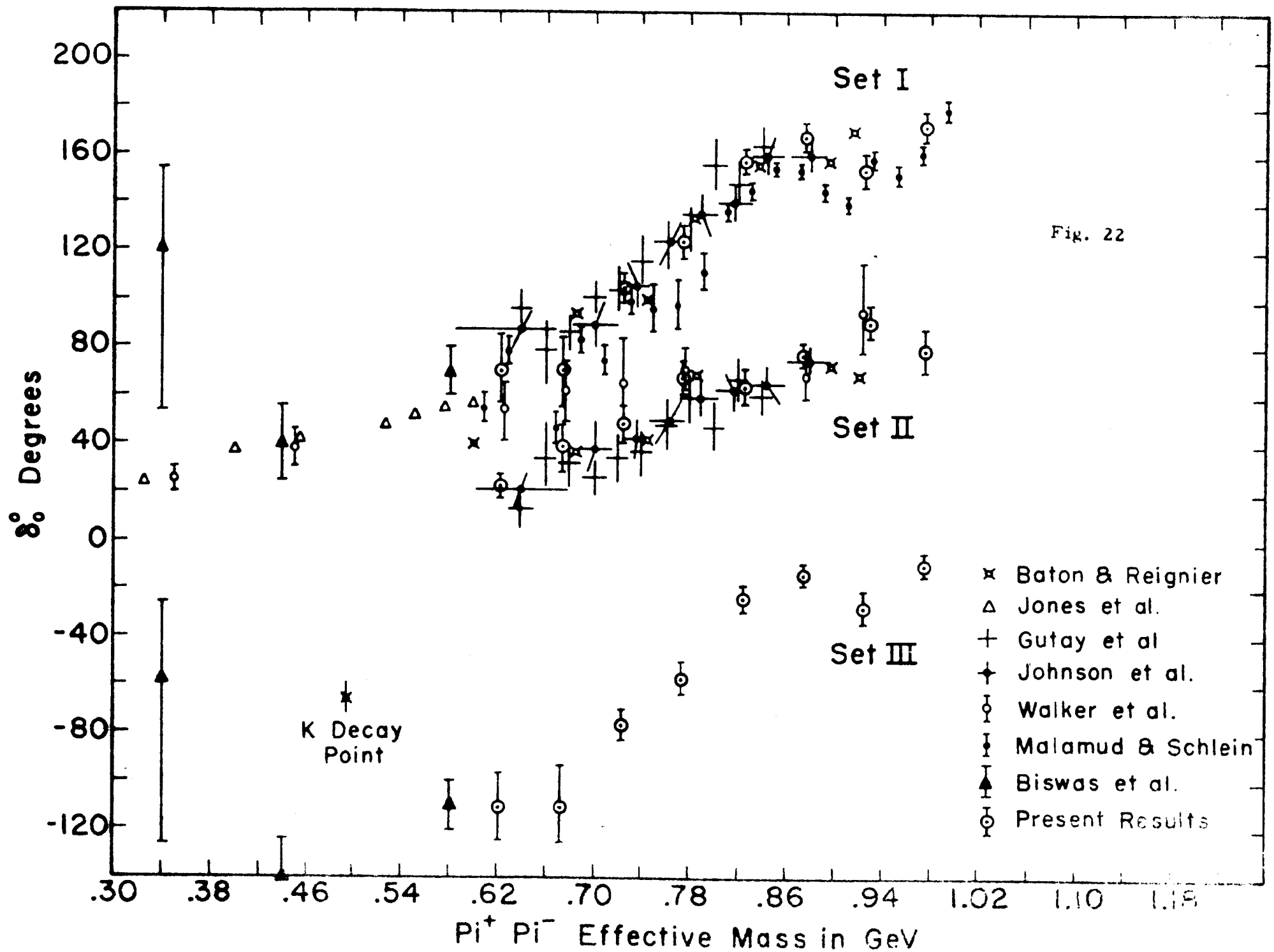


Fig. 22

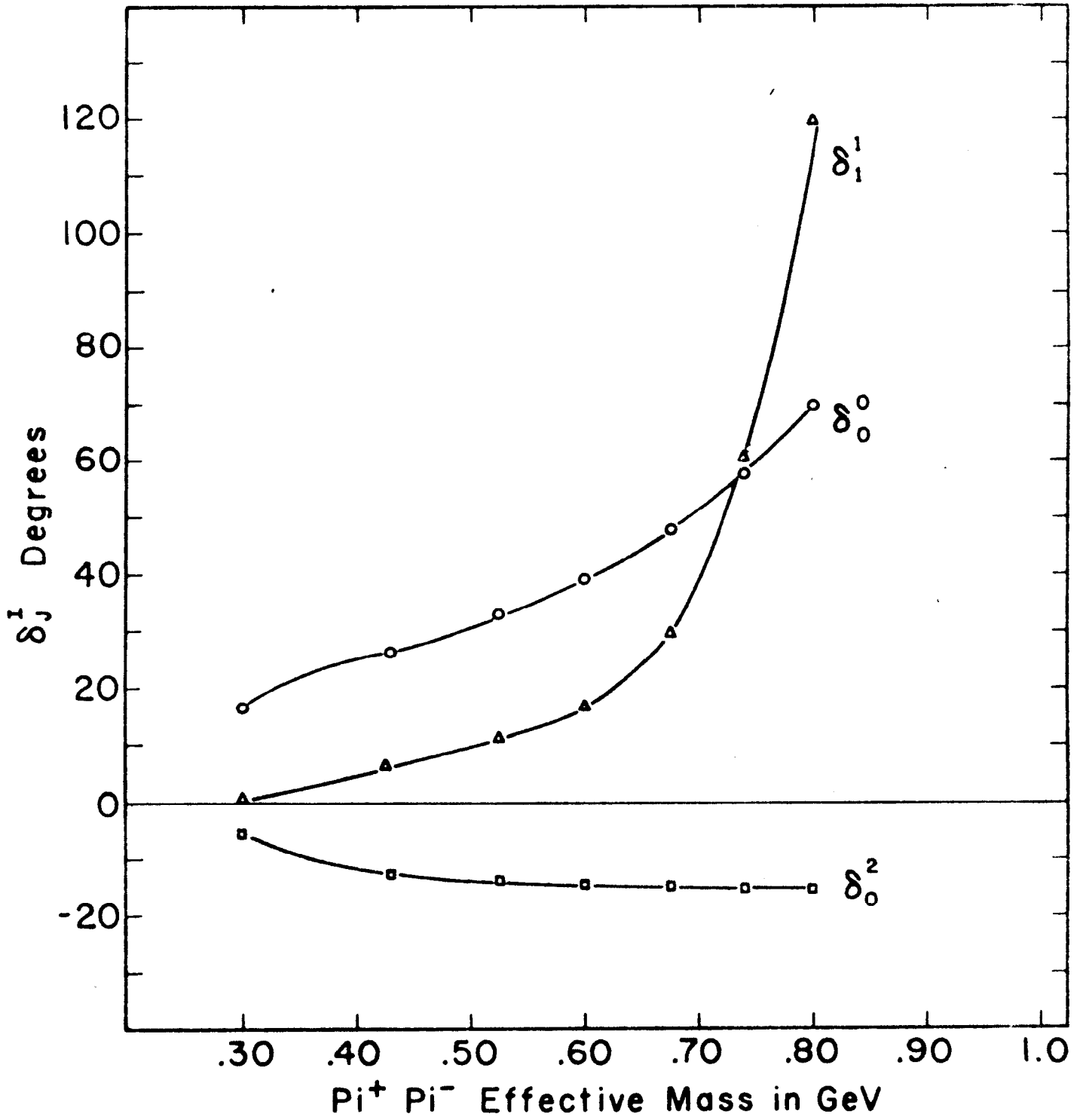


Fig. 23

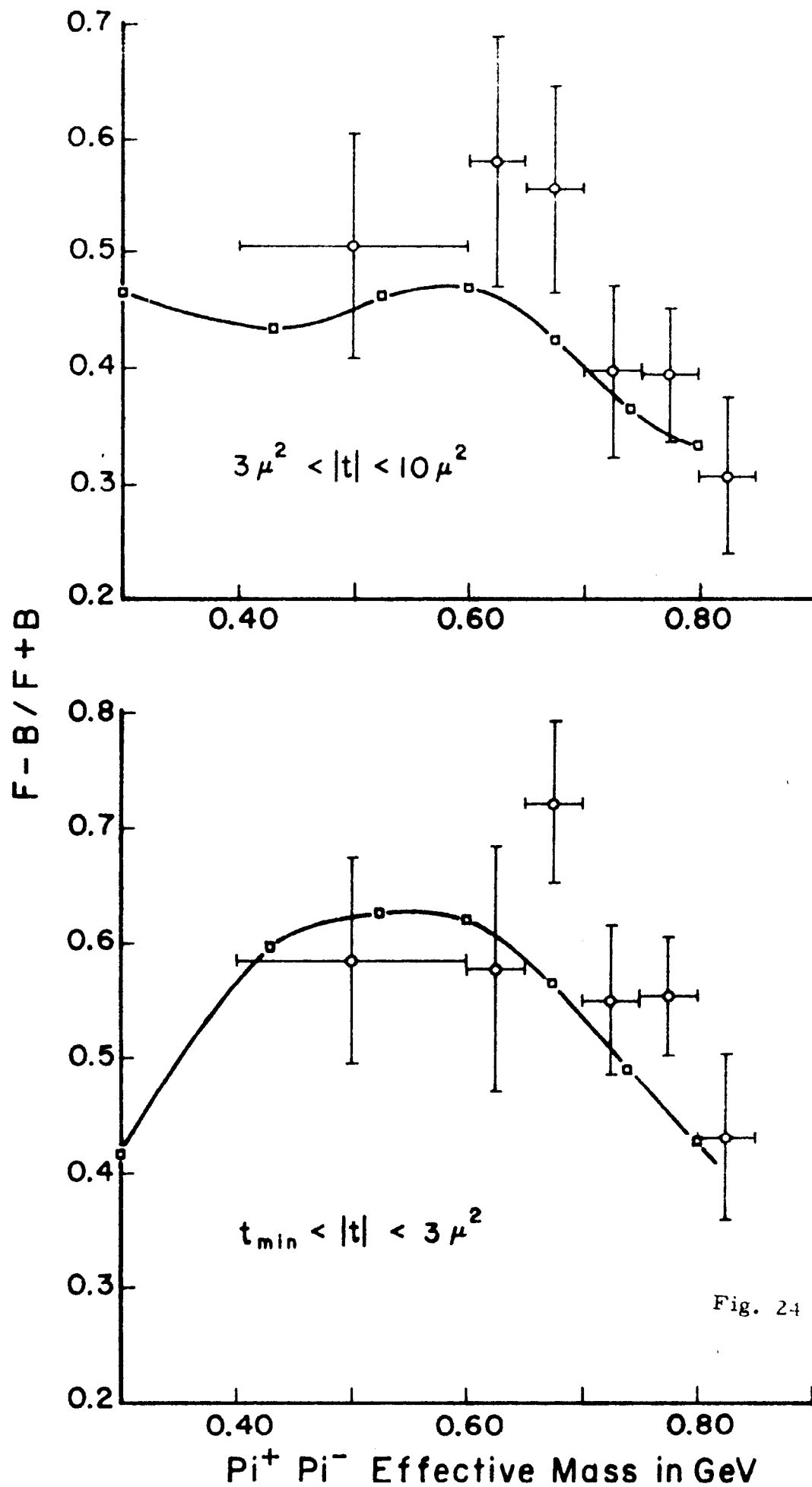


Fig. 24

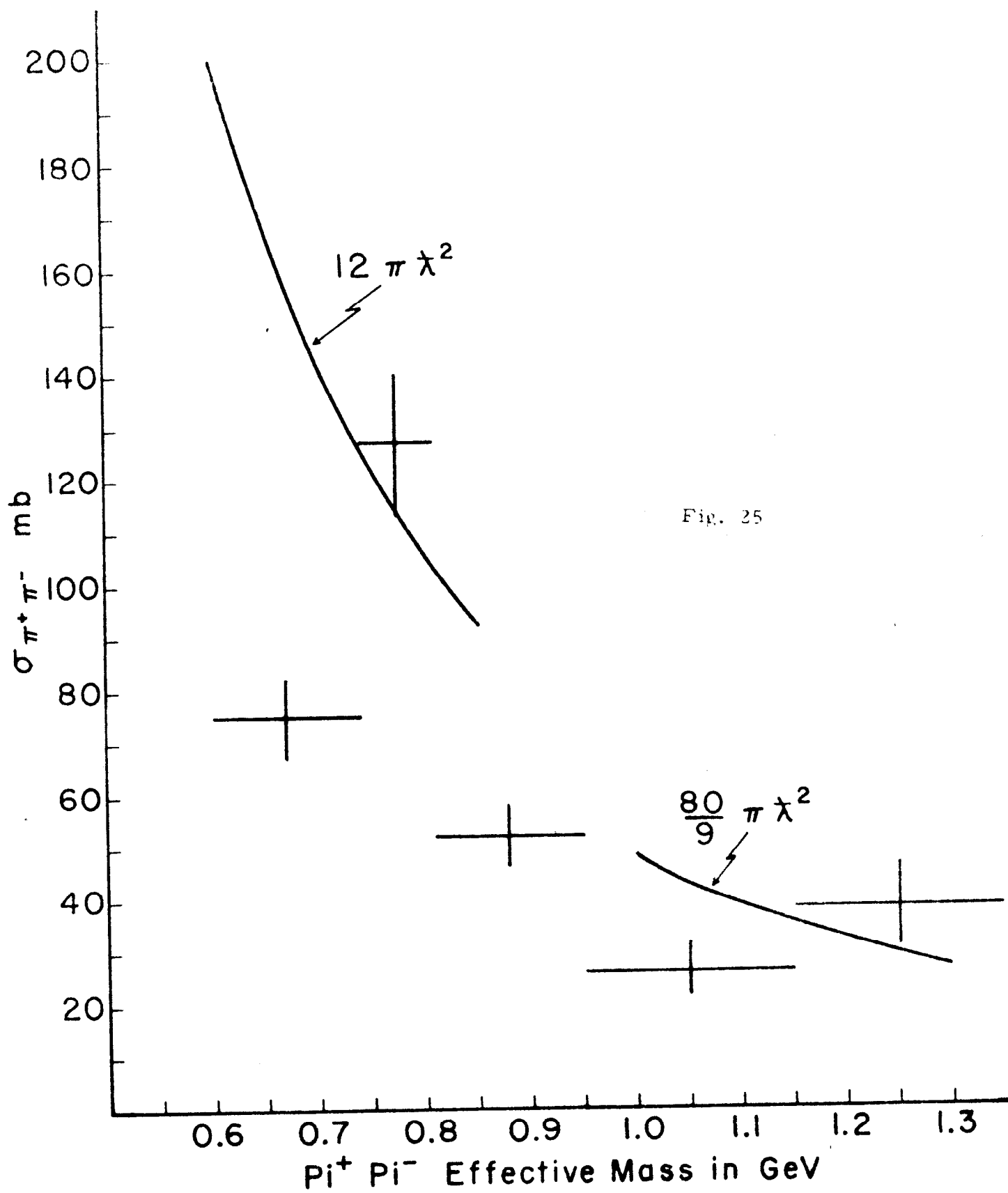


Fig. 25

# Legendre Coefficients For $t \leq .2$ (GeV/c)<sup>2</sup>

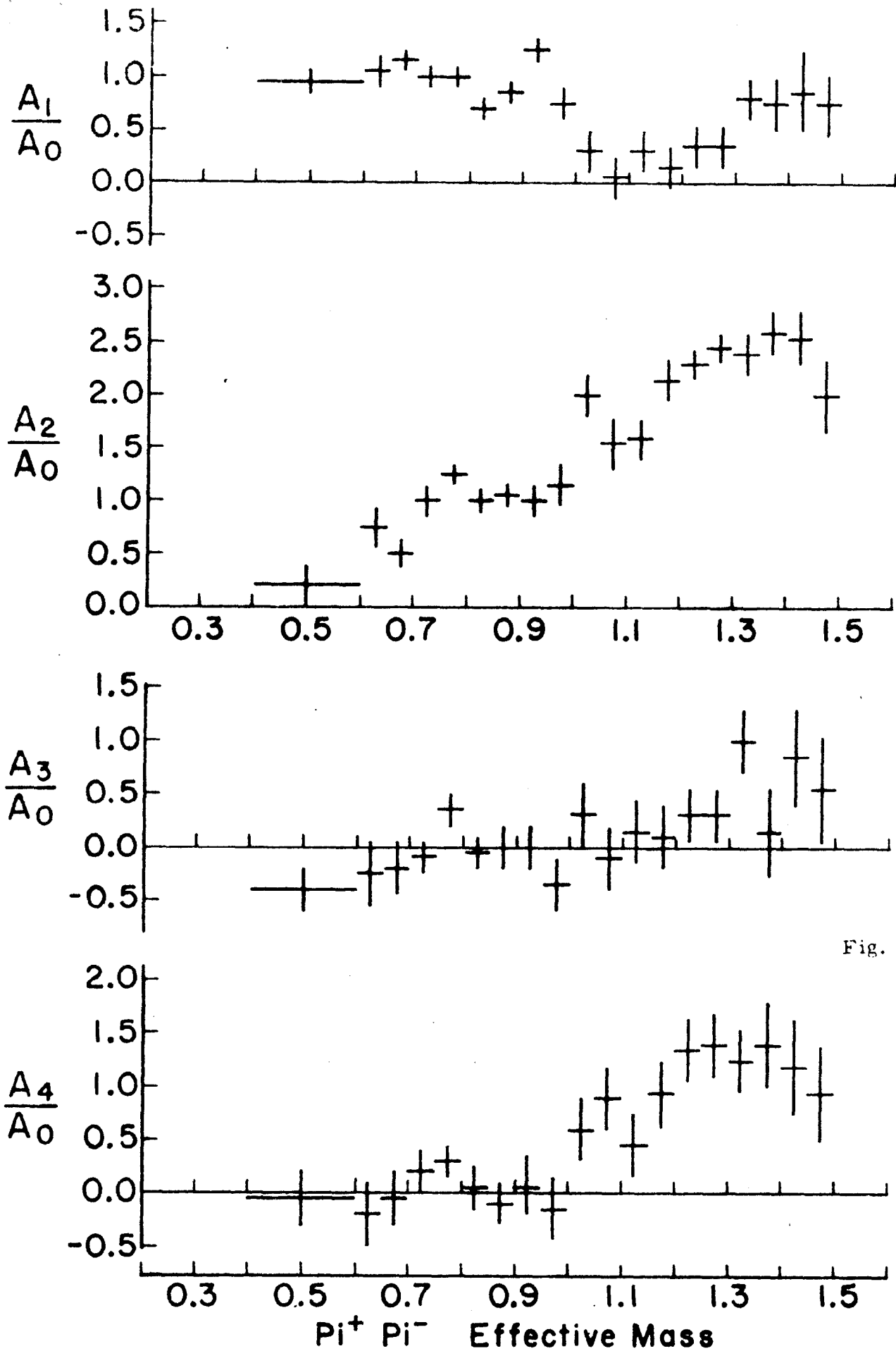


Fig. 26

Legendre Coefficients For  $l \leq 4$  ( $\text{GeV}/c$ )

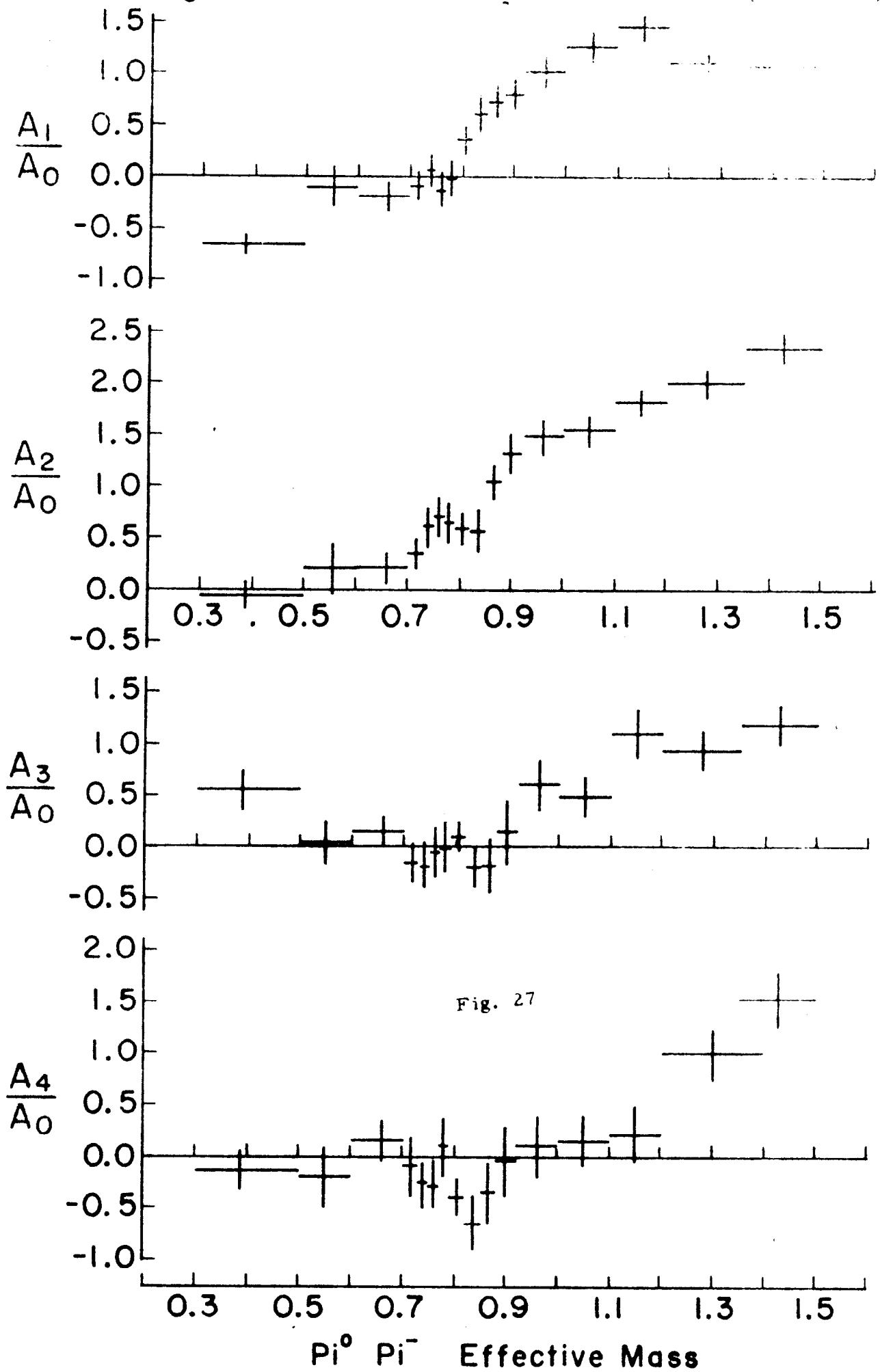


Fig. 27

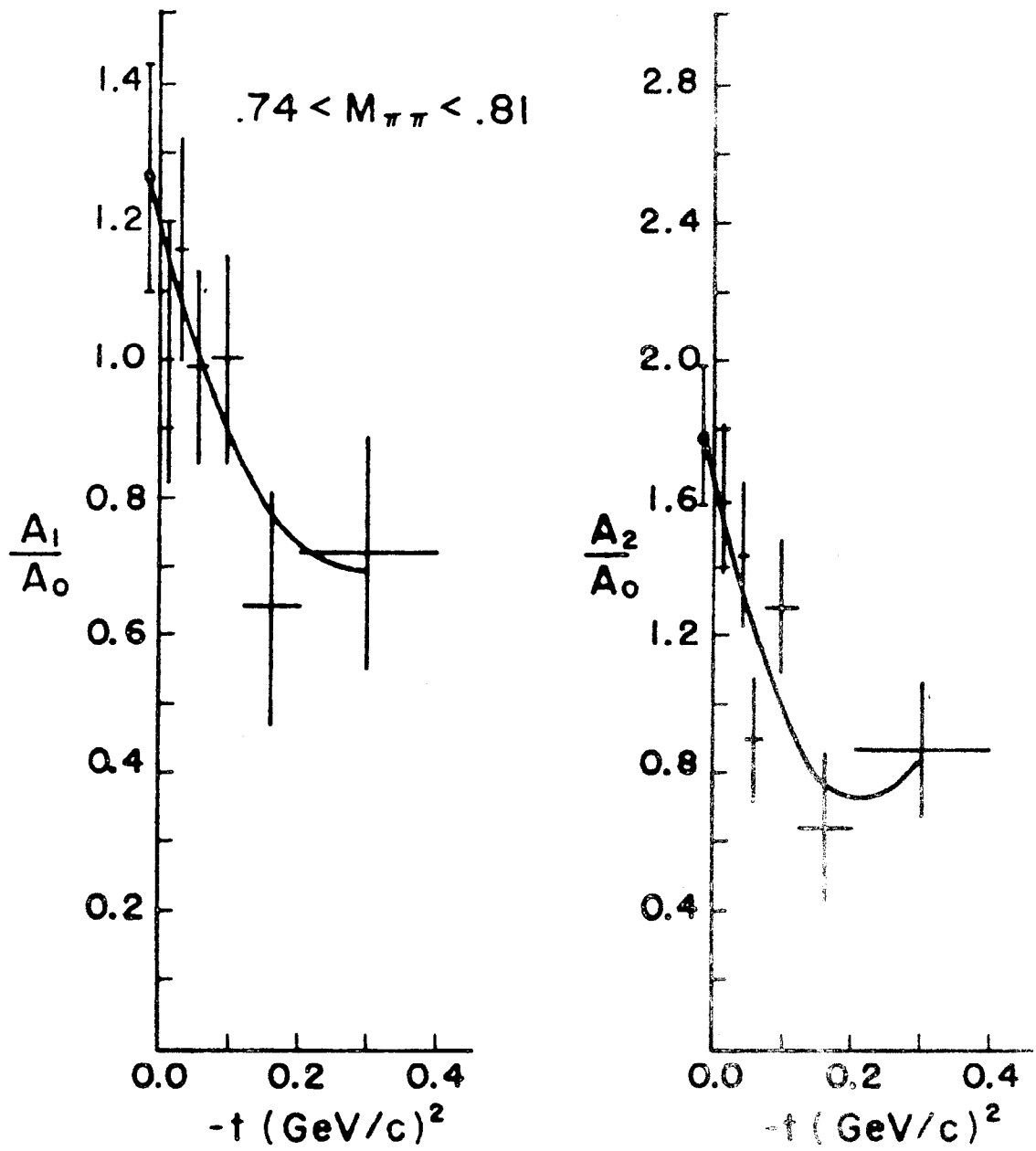


Fig. 28